Mechanism of CO_2 and NH_3 Transport through Human Aquaporin 1: Evidence for Parallel CO_2 Pathways

Raif Musa-Aziz[1,2*‡], R. Ryan Geyer[2*], Seong-Ki Lee[2], Fraser J. Moss[2], and Walter F. Boron[2,3,4‡]

[1]Department of Physiology and Biophysics, Institute of Biomedical Sciences, University of Sao Paulo.
[2]Department of Physiology and Biophysics, [3]Department of Medicine, and [4]Department of Biochemistry
Case Western Reserve University School of Medicine
Cleveland, OH 44106, USA.

Key words: *CO_2 permeability, osmotic water permeability, Surface pH, Xenopus laevis oocytes*
Running Title: *CO_2 pathways through AQP1*
For submission to: *The Journal of Physiology*

Author Contacts:

Raif Musa-Aziz
Department of Physiology and Biophysics
Institute of Biomedical Sciences
University of Sao Paulo
Sao Paulo, SP Brazil
Tel: 55-11-3091-7281
E-mail: raifaziz@icb.usp.br

R Ryan Geyer
E-mail: geyerro1976@gmail.com

*These authors contributed equally to this work

‡ **Address correspondence to:**

Raif Musa-Aziz
Department of Physiology and Biophysics
Av. Prof Lineu Prestes, 1524,
Sao Paulo, SP, Brazil 05508-000
Tel: 55-11-3091-7281
E-mail: raifaziz@icb.usp.br

Walter F. Boron
Department of Physiology and Biophysics
10900 Euclid Ave. Robbins Building E524
Cleveland, OH, USa 44106-4970
Tel: 1-216-368-8978
E-mail: walter.boron@case.edu

38 ## Key Points

39 • Some membranes have little or no CO_2 permeability, absent protein channels like
40 aquaporin-1 (AQP1).

41 • We confirm that, during CO_2 influx, heterologous expression of human AQP1 (hAQP1) in
42 *Xenopus* oocytes increases the magnitude of the transient surface-pH increase by an
43 amount $(\Delta pH_S^*)_{CO_2}$, measured with microelectrodes. During NH_3 influx, hAQP1
44 expression increases the magnitude of the transient pH_S decrease by $(\Delta pH_S^*)_{NH_3}$.

45 • p-chloromercuribenzene sulfonate (pCMBS), which reacts with C189 in the monomeric
46 pore, reduces $(\Delta pH_S^*)_{CO_2}$ by; $(\Delta pH_S^*)_{NH_3}$, to zero; and AQP1-dependent osmotic water
47 permeability (P_f*), by half.

48 • 4,4'-diisothiocyanatostilbene-2,2'-disulfonate (DIDS) reduces $(\Delta pH_S^*)_{CO_2}$ by half, but has
49 no effect on $(\Delta pH_S^*)_{NH_3}$ or P_f*. DIDS crosslinks AQP1 monomers expressed in *Pichia*
50 *pastoris*.

51 • Together, pCMBS+DIDS reduces $(\Delta pH_S^*)_{CO_2}$ to zero. The C189S mutation of AQP1
52 eliminates the effects of pCMBS, but not DIDS. Our results thus show that CO_2 traverses
53 AQP1 via the monomeric pore plus a novel, DIDS-sensitive route that may be the central
54 pore.
55

Abstract

The traditional view had been that dissolved gases cross membranes simply by dissolving in and diffusing through membrane lipid. However, some membranes are impermeable to CO_2 and NH_3, whereas some aquaporin (AQP) water channels—tetramers with hydrophobic central pores—are permeable to CO_2, NH_3, or both. Nevertheless, we understand neither the routes that CO_2 and NH_3 take through AQP tetramers, nor the basis of CO_2/NH_3 selectivity. Here, we show—for human AQP1 (hAQP1)—that virtually all NH_3 and H_2O pass through the hydrophilic, monomeric pores. However CO_2 passes both through the monomeric pores and another pathway. We expressed hAQP1 in *Xenopus* oocytes and used microelectrodes to monitor the maximal surface-pH transient (ΔpH_S) caused by CO_2 or NH_3 influxes. We found that p-chloromercuribenzene sulfonate (pCMBS)—which reacts with C189 in the monomeric pore—eliminates the entire hAQP1-dependent (*) NH_3 signal $(\Delta pH_S^*)_{NH_3}$, but only half of the signals for CO_2 $(\Delta pH_S^*)_{CO_2}$ or osmotic water permeability P_f^*. 4,4'-diisothiocyanatostilbene-2,2'-disulfonate (DIDS), eliminates the remaining $(\Delta pH_S^*)_{CO_2}$ but has no effect on $(\Delta pH_S^*)_{NH_3}$ or P_f^*. Together, the two drugs completely eliminate the CO_2 permeability of hAQP1. When we express hAQP1 in *Pichia pastoris*, treat spheroplasts with DIDS, and examine hAQP1 by SDS-PAGE, reactivity with an anti-DIDS antibody shows that DIDS crosslinks hAQP1 monomers. Our results provide the first evidence that a molecule can move through an AQP via a route other than the monomeric pore, and raise the possibility that selectivity depends on the extent to which CO_2/NH_3 move through monomeric pores vs. an alternate pathway (e.g., the central pore).

76 # Introduction

77 Before the discovery of specific protein-mediated pathways in cell membranes, investigators
78 had believed that many small molecules (e.g., H_2O, urea, glycerol, lactic acid)—including CO_2—
79 freely permeate all membranes to the extent that they can dissolve in and then diffusing through
80 the lipid phase. Solubility-diffusion theory (S-DT) embodies this concept (reviewed in Boron,
81 2010; Michenkova *et al.*, 2021). For molecules other than dissolved gases, the generalizability of
82 this notion faded with the discovery of each new membrane channel or transporter, consistent with
83 the idea that cells evolved to achieve tight control over the transmembrane traffic of small
84 molecules. We now believe that the traffic of such molecules depends on some combination of
85 membrane proteins and S-DT (responsible for non-specific leaks).

86 Regarding CO_2 traffic across biological membranes, the first inconsistency in the applicability
87 of S-DT was the demonstration that apical membranes (i.e., facing the lumen) of single gastric
88 glands are impermeable to CO_2 (Waisbren *et al.*, 1994). The second was the discovery that the
89 human (h) aquaporin-1 (AQP1) not only conducts H_2O of course (Preston & Agre, 1991), but also
90 CO_2 (Nakhoul *et al.*, 1998). Soon after Nakhoul's observation, Cooper and Boron (1998) found
91 that pCMBS inhibits CO_2 permeability in oocytes expressing wild-type (WT) hAQP1. Prasad *et*
92 *al.* (1998) then reported that AQP1 purified from human red blood cells (RBCs) and reconstituted
93 into lipids from *E. coli* increases CO_2 permeability, an effect blocked by $HgCl_2$. Moreover, Forster
94 *et al.* (1998) found that 4,4'-diisothiocyanatostilbene-2,2'-disulfonate (DIDS) applied to native
95 human RBCs reduces not only HCO_3^- permeability, but also CO_2 permeability.

96 Forster and colleagues recognized that an explanation for their data could be that DIDS blocks
97 a protein pathway for CO_2 diffusion through the RBC membrane. Indeed, Endeward *et al.* (2006)
98 later found that AQP1 is responsible for about half of the CO_2 traffic across the human RBC
99 membrane, with the rhesus (Rh) complex's being responsible for most of the rest (Endeward *et*
100 *al.*, 2008), leaving <10% to be accounted for by S-DT. Uehlein *et al.* (2003) reported that NtAQP1
101 in tobacco plants plays important physiological roles in CO_2 uptake—driven by a very small air-
102 to-chloroplast gradient—for photosynthesis, stomatal opening, and leaf growth. Wang and
103 colleagues demonstrated that the CO_2 permeability of tomato aquaporin PIP2;1 is essential for
104 CO_2-dependent regulation of stomatal aperture (Wang *et al.*, 2016).

105 Besides H_2O and CO_2, various AQPs can conduct a variety of substances, including glycerol
106 in the case of members of the aquaglyceroporin subfamily (Gomes *et al.*, 2009). Regarding

107 dissolved gases, hAQP1 conducts NH_3 (Nakhoul *et al.*, 2001) and NO (Herrera *et al.*, 2006).
108 Moreover, different AQPs can exhibit strong selectivity for CO_2 over NH_3 or vice versa (Musa-
109 Aziz *et al.*, 2009*a*; Geyer *et al.*, 2013). More recent work has suggested that *Nicotiana tabacum*
110 PIP1;3 (Zwiazek *et al.*, 2017) as well as hAQP1 (Al-Samir *et al.*, 2025) are permeable to O_2, and
111 that AQP1, the Rh complex, and an unidentified protein are responsibly for nearly all O_2
112 permeability in murine RBCs (Moss *et al.*, 2025; Occhipinti *et al.*, 2025; Zhao *et al.*, 2025). These
113 results are consistent with the idea that cells, by regulating channel expression and trafficking to
114 specific membranes, could control the permeability to CO_2, O_2, and NH_3.

115 Structural studies show that AQP1 is a homotetramer with four independent monomeric
116 pores—lined mainly by hydrophilic residues—that conduct H_2O (Walz *et al.*, 1997; Sui *et al.*,
117 2001). At the core of its square-shaped array of four monomers, AQP1 has a central pore—lined
118 exclusively by hydrophobic residues—with no established function. Each monomer spans the lipid
119 bilayer six times and has cytoplasmic amino and carboxyl termini. As predicted by the "hourglass
120 model" of Preston and Agre (1991), two consensus NPA motifs—on intracellular and extracellular
121 loops that dip in towards the middle of AQP1, near the plane of the membrane—contribute
122 importantly to the monomeric pore. The well-established reduction of osmotic water permeability
123 (P_f) by $HgCl_2$ or pCMBS occurs as these agents react with cysteine-189 (C189), two residues
124 upstream from the second NPA (Preston *et al.*, 1993). Replacing this cysteine with serine (C189S),
125 which lacks a sulfhydryl group, eliminates this inhibition (Preston *et al.*, 1993).

126 We previously introduced an approach for using blunt, pH-sensitive microelectrodes to
127 monitor transient changes in extracellular-surface pH (pH_S), caused by the entry of CO_2 or NH_3
128 into *Xenopus* oocytes heterologously expressing membrane proteins (Endeward *et al.*, 2006; Musa-
129 Aziz *et al.*, 2009*b*, 2009*a*, 2010, 2014*a*). Mathematical modeling has elucidated the interpretation
130 of CO_2-dependent pH_S transients (Somersalo *et al.*, 2012; Occhipinti *et al.*, 2014; Calvetti *et al.*,
131 2020). Using this pH_S approach in a survey of mammalian AQPs, we found that AQPs 1, 6, and 9
132 are permeable to both CO_2 (exposure to 5% CO_2) and NH_3 (0.5 mM NH_4Cl); AQP0, the M23
133 variant of AQP4 (AQP4-M23), and AQP5 are permeable to CO_2 but not NH_3; AQPs 3, 7, and 8
134 are permeable to NH_3 but not CO_2; and AQP2 as well as AQP4-M1 appear to be permeable to
135 neither (Musa-Aziz *et al.*, 2009*a*; Geyer *et al.*, 2013). Using an osmotic-shrinkage assay with an
136 80-fold higher extracellular [NH_3] than in our studies, Assentoft et al detected NH_3 permeability
137 through AQP4-M23 (Assentoft *et al.*, 2016). A key unanswered question is how various AQPs

138 exhibit such strikingly different CO_2/NH_3 selectivities. The answer presumably lies in the
139 pathways that these solutes take through various AQP tetramers. However, despite insights from
140 molecular-dynamics simulations (Wang *et al.*, 2007; Assentoft *et al.*, 2016), we still lack
141 physiological evidence that establishes the pathways by which either CO_2 or NH_3 moves through
142 any AQP. The purpose of the present study is to explore this problem.

143 Our approach was to use a combination of cell physiology and biochemistry. Heterologously
144 expressing hAQP1 or its C189S mutant in *Xenopus* oocytes, and using the pH_S approach, we
145 assessed the effects of pCMBS and DIDS on CO_2 and NH_3 permeation. We also assessed P_f so
146 that we could normalize CO_2 and NH_3 data to H_2O permeability. We examine pCMBS because
147 mercury—acting on monomeric pores—reduces both the P_f (Preston *et al.*, 1993) and CO_2
148 permeability of hAQP1 (Cooper & Boron, 1998), as expressed heterologously in oocytes. We work
149 with DIDS because this drug reduces CO_2 permeability in RBCs, and in oocytes expressing hAQP1
150 (Endeward *et al.*, 2006). We find that virtually all of the hydrophilic NH_3 molecules—as well as
151 H_2O, as expected—pass through the four hAQP1 monomeric pores, which each possess three
152 hydrophilic nodes in their selectivity filters that are located at the center of an otherwise long
153 hydrophobic channel (Sui *et al.*, 2001). On the other hand, the more hydrophobic CO_2 travels both
154 via this pCMBS-sensitive pathway—the only established pathway through any AQP—as well as
155 an independent pathway that we can block with DIDS. Studies on hAQP1 expressed in *Pichia*
156 *pastoris* indicates that DIDS crosslinks hAQP1 monomers. Our work is the first to demonstrate
157 that a substance can move through an AQP via a pathway—possibly the hydrophobic central
158 pore—that is distinct from the monomeric pore. Considering that mutations in human AQPs are
159 associated with a wide variety of pathological conditions (see (Verkman, 2008; Verkman *et al.*,
160 2008; Wang & Boron, 2025), our work could lead to new insights into disease mechanisms,
161 diagnostic tools, and therapeutic approaches for improving clinical outcomes.

Methods

For previous summaries of our approach in oocyte experiments, see Musa-Aziz et al. (2010, 2009a, 2009b). The following description is in greater depth.

Ethical approval and animal procedures

The Institutional Animal Care and Use Committee at Case Western Reserve University approved the protocols for housing and handling of *Xenopus laevis* (approval #2020-0066), used as a source of oocytes, and rabbits (approval # 2010-0146), for generating polyclonal antibodies.

Frogs. We purchased adult female *Xenopus laevis* frogs (NASCO Inc., Fort Atkinson, WI, USA) and housed them in a 20-gallon static aquarium, managed by the Animal Resources Center (ARC) of the School of Medicine. For stress mitigation, the tank had six or fewer frogs, and for environmental enrichment, we included a PVC elbow pipe. A charcoal Bio-Bag aquarium power pump (Tetra, Blacksburg, VA) circulated dechlorinated water through the tank. Three times per week, ARC staff fed the frogs with adult *Xenopus* diet (Zeigler Bros. Inc., Gardners, PA), sprinkling the food (10 pellets/frog) into the tank and, after a few hours when the *Xenopus* had fed, removing excess food with a net. As judged necessary, the ARC staff partially changed out water in the tank. Every 90 days, they moved the frogs into a newly cleaned tank that contained, in equal amounts, water from the previous tank and new de-chlorinated water.

We anesthetized frogs by immersion in a solution containing 0.2% tricaine (i.e., MS-222; ethyl 3-aminobenzoate methanesulfonate, catalog # A5040, Sigma-Aldrich, St Louis, MO, USA). When an animal became unresponsive to touch, we removed it from the solution and surgically extracted the ovaries. The animal was euthanized by cardiac excision prior to recovery from anesthesia.

In some experiments, we isolated oocytes from *Xenopus* ovarian lobes shipped overnight from NASCO.

Rabbits. We purchased adult female New Zealand white rabbits [1] from Charles River Laboratories (Ashland, OH). Following IACUC guidelines, ARC staff obtained a 5-mL pre-immune blood sample from an ear vein, and then inoculated two rabbits—gently restrained in a

[1] We code-named the rabbits, and the antisera they produced, “Ren” and “Stimpy.”

188 rabbit-restraint cage, and lightly sedated with intramuscular acepromazine (2 mg/kg)—with fresh
189 DIDS-KLH fusion protein (see below) and Freund's complete adjuvant via subcutaneous injection
190 on the back of the rabbit. A 10-mL sample of blood (via ear veins, alternating sides) was taken 14–
191 21 days after the first boost, and the sera were evaluated for antigenicity towards proteins labeled
192 with DIDS. Once a rabbit began producing sufficient titers of polyclonal anti-DIDS antibodies,
193 staff collected 10 mL of blood per kg of body weight (~30–50 mL) at intervals of 21 to 30 days.
194 After two of such larger blood collections, ARC staff euthanized the animals by cardiac excision
195 and exsanguination, with blood from the terminal collection being transferred to our laboratory.

196 Solutions and chemicals

197 **OR3 media (for maintaining oocytes).** We follow the protocol described in (Musa-Aziz *et*
198 *al.*, 2010). Briefly, we added to 1.8 L of H_2O one pack of powdered Leibovitz L-15 media with L-
199 glutamine (catalog # L4386, Sigma-Aldrich), 100 mL of 10,0000 U/mL penicillin/streptomycin
200 solution (cat # 15140122, Thermo Fisher Scientific, Waltham, MA, USA; hereafter abbreviated
201 TFS) and 5 mM HEPES free acid. We then titrated the solution to pH 7.50 with NaOH,
202 periodically measuring osmolality 195 mOsm, and sterile-filtered the solution using a Corning™
203 Disposable Vacuum Filter/Storage system (catalog # 09-761-107, TFS), and stored it in a cold
204 room for up to 2 weeks before use. Finally, just before use, we sterile-filtered a small volume of
205 solution using a 60-mL syringe (catalog # 14-955-461, TFS) and a sterile in-line Nalgene filter
206 with a 0.22-μm pore size and a 25-mm diameter (catalog # 723-9920, TFS).

207 **Solutions for physiology experiments.** Table 1 describes the final composition of nine
208 solutions used in the physiology experiments. All were assembled and used at room temperature
209 (~22°C). Where necessary, we describe any necessary additional steps for correct solution
210 assembly (e.g. the order in which components should be added) below.

211 **(Solution 3) 5% CO_2/33 mM HCO_3^- for measuring ΔpH_S due CO_2 influx).** After adding all
212 components except $NaHCO_3$, we titrated the solution to pH 7.50, then added the 33 mM $NaHCO_3$,
213 and then equilibrated the solution with 5% CO_2 (balance with air), which brought pH back to 7.50.

214 **(Solutions 4 and 5) 0.5 mM NH_3/NH_4^+ in ND96 (for measuring ΔpH_S due NH_3 influx).** We
215 first made the 5 mM NH_3/NH_4^+ in ND96 solution (Solution #4) in which we replaced 5.0 mM NaCl
216 with an equivalent amount of NH_4Cl, and then diluted this solution 1:10 into ND96.

217 **(Solution 6) Hypotonic ND96 (for measuring P_f):** This is a variant of ND96 in which we
218 reduced [NaCl] to lower osmolality to 80 mOsm/kg.

219 **(Solution 7) ND96 + pCMBS.** In some experiments, we pre-incubated oocytes for 30 min in
220 an ND96 containing 1 mM pCMBS (catalog # C367750, Toronto 196 Research Chemicals, North
221 York, Ontario, Canada), a sulfhydryl reagent, added to solution as dry powder to ND96 (Solution
222 #1).

223 **(Solution 8) DIDS.** In some experiments, we pre-incubated oocytes for 1 h in an ND96
224 containing 100 μM DIDS (catalog # D3514, Sigma-Aldrich), an amino-reactive agent added to the
225 solution as a dry powder to ND96 (Solution #1).

226 **(Solution 9) BSA (Bovine serum albumin, to scavenge DIDS).** In some experiments, after
227 DIDS pretreatment, we washed off un-reacted DIDS by exposing oocytes to an ND96 to which we
228 added 0.2% BSA (catalog # A9418, Sigma-Aldrich) directly to ND96 (Solution #1).

229 When assembling all solutions, we measured pH using a Ross electrode (catalog # 927007MD,
230 TFS), a Dual Star pH meter (catalog # 8102BNUWP, TFS), and calibrated with two standards
231 (from TFS), buffer solution pH 6.0 (catalog # SB104-1) and 8.0 (catalog # SB112-20). We
232 measured osmolality with a vapor-pressure osmometer (catalog # 5520 Vapro, Wescor Inc.,
233 Logan, UT).

234 Oocyte Isolation

235 We placed ovarian lobes in a sterile 100-mm Petri dish containing ND96, cut them into
236 irregular pieces (<1 cm on an edge) containing ~10 oocytes each using small iridectomy scissors,
237 poured the mixture into a new Petri dish containing ~15 mL of Ca^{2+}-free ND96, gently agitated
238 the dish on a horizontal shaker[2] for 10 min, poured off as much liquid as possible, added fresh
239 Ca^{2+}-free ND96, and repeated the pour/shake/wash cycle twice more. We then poured off the Ca^{2+}-
240 free ND96, before adding ~15 mL of a freshly-made mixture of Ca^{2+}-free ND96 and 2 mg/mL
241 Collagenase Type IA (catalog # C9722, Sigma-Aldrich), and gently agitating the dish on a
242 horizontal shaker for 40 min. We next poured off the collagenase solution, added collagenase-free

[2] In some later experiments, we instead put the oocytes and Ca^{2+}-free solution into 50-mL Falcon tubes (catalog # 14-959-49A, TFS) and agitated them using a Tube Rotator (Scientific Equipment Products, Baltimore, MD).

243 Ca^{2+}-free ND96, gently agitated the dish for 15 min, and repeated the pour/shake/wash cycle twice
244 more. We then poured off the Ca^{2+}-free ND96, added ND96 (i.e., containing Ca^{2+}), gently agitated
245 the dish on a horizontal shaker for 15 min, and repeated the pour/shake/wash cycle twice more.
246 Finally, we poured off the ND96, added ~15 mL OR3 media, repeated the pour/wash cycle twice
247 more, poured off most of the liquid, transferred the oocytes and remnant OR3 media to a fresh
248 petri dish containing fresh OR3 media, and incubated the oocytes in an incubator at 18ºC. Later
249 the same day, we used a stereomicroscope to sort the oocytes and select individual, defolliculated,
250 mature oocytes (stage V/VI), which we immediately moved to a 6-well plate containing OR3
251 media (as many as ~50 oocytes/well), using a fire-sterilized transfer pipette prepared by using a
252 diamond pencil to score the tapered end of a Pasteur pipette at a diameter large enough to
253 accommodate an oocyte, breaking off and discarding the thin end of the pipette, fire-polishing the
254 cut end of the pipette, and attaching the large end of the pipette to a manual, 2-mL Pipette Pump
255 pipetter (catalog # S3-594-3, TFS). We incubated the oocytes overnight at 18ºC before injection
256 the following day with cRNA or H_2O (see below).

257 cRNA synthesis

258 The cDNAs encoding both hAQP1-WT (accession# NM_198098) and AQP1-C189S were
259 gifts of Dr. Peter Agre (Johns Hopkins University). We subcloned the open reading frames of the
260 constructs into the expression plasmid pGH19 (Trudeau *et al.*, 1995), a vector containing the 3′
261 and 5′ untranslated regions of the *Xenopus* laevis β-globin gene. In experiments in which we
262 expressed AQP1-WT or AQP1-C189S in *P. pastoris*—as well as in some control experiments in
263 oocytes—we added an N-terminal (Nt) FLAG-tag (MDYKDDDDKASEFKKKL… ; FLAG
264 sequence, underscored; AQP1 sequence, double underscored).

265 We linearized cDNA constructs using NotI (for untagged AQP1-WT and AQP1-C189S) or
266 XhoI (for the AQP1-FLAG tagged versions). The linearized DNA was then purified using the
267 QIAquick PCR purification kit (catalog # 28104, Qiagen Inc., Valencia, CA). We then synthesized
268 capped RNA (cRNA) using T3 (for untagged constructs; catalog# AM1348, Ambion, Austin, TX,
269 USA) or T7 (for FLAG-tagged constructs; catalog# AM1344, Ambion) mMessage mMachine kits
270 (Ambion, Austin, TX, USA). The cRNA was purified using the RNeasy MinElute RNA Cleanup
271 Kit (catalog # 74204, Qiagen). The cRNA concentration was determined based on ultraviolet
272 absorbance at 260 nm, and quality was assessed according the A260/280 ratio and gel
273 electrophoresis.

274 ## Injection of oocytes with cRNA or water

275 One day after isolation and defolliculation, we injected stage V–VI oocytes with 25 nL of
276 cRNA (1 ng/nL) encoding AQP1-WT, its C189S mutant, or the FLAG-tagged versions, or ~25 nL
277 of water as a control. The injection apparatus consisted of a Nanoject II Variable Volume
278 Automatic Injector (Drummond Scientific Company, Broomall, PA) connected to an injection
279 needle that we pulled from 10-µl microdispenser capillary glass tubing (catalog # 3-000-210-G,
280 Drummond), using a Model P-97 Flaming/Brown Micropipette Puller (Sutter Instrument
281 Company, Novato, CA) and then modified by manually breaking the sealed end to yield a tip
282 diameter of ~50-µm. After injection, we transferred oocytes to a 6-well plate (up to ~50/well) and
283 incubated in OR3 media and maintained them for 3 days in an incubator at 18 °C before use.

284 ## Electrophysiological recordings

285 For a schematic representation of the experimental chamber, position of the oocyte, and
286 arrangement of electrodes, see figure 8b in Musa-Aziz *et al.* (2010).

287 **Chamber and solution delivery.** We placed oocytes into the channel (3 mm wide × 2 mm
288 deep × 30 mm long) of a plastic perfusion chamber. We delivered the physiological solutions—or
289 pH standards for calibrating pH microelectrodes at the outset of an experiment (see next section)—
290 at a constant, total flow of 4 mL/min at room temperature (~22 °C), using a series of dual-syringe
291 pumps (Model 22, Harvard Apparatus, South Natick, MA), each of which drove two 140-mL
292 plastic syringes (Sherwood Medical, St. Louis, MO) of identical content to deliver two solutions
293 at 2 mL/min each.[3] The two solutions from each pump flowed through separate lengths of Tygon
294 tubing (5/32-inch (~4.0 mm) outer diameter, 3/32-inch (~2.4 mm) inner diameter; Ryan Herco
295 Products Corp., Burbank, CA; Formulation R3603-3; OD 4.8 mm /ID 1.6 mm) to two parallel
296 assemblies of pneumatically operated 5-way valves (Clippard Instrument Laboratory, Cincinnati,
297 OH), daisy-chained in such a way that we could switch among identical pairs of solution lines.
298 The output of the parallel switching assemblies flowed into two lengths of Tygon tubing that
299 carried the solutions to the vicinity of the chamber, where the two lines merged in a "mixing T",

[3] We apparatus had this dual-solution arrangement to enable the use of out-of-equilibrium CO_2/HCO_3^- solutions in experiments that are not part of the present study.

300 the output of which flowed into one end of the chamber channel. A suction device removed the
301 solution at the opposite end of the channel. See Musa-Aziz *et al.* (2014) for details.

302 **Measurement of membrane potential and intracellular pH.** As described previously (Musa-
303 Aziz *et al.*, 2010, 2014*a*), we impaled the oocyte (with the dark animal pole facing upward) with
304 two microelectrodes, one for measuring membrane potential and the other for measuring
305 intracellular pH. Both microelectrodes, with tip diameters of ~1 μm, we pulled from thin-walled
306 borosilicate microfilament glass tubing (Catalog # G200TF-4, 2.0 mm OD ×1.56 mm ID, Warner
307 Instruments Corporation, Hamden, CT), using the aforementioned P-97 microelectrode puller.

308 The microelectrodes for measuring membrane potential (V_m) we filled with 3 M KCl. We
309 inserted an electrode into a half-cell/microelectrode holder (model # ESW-F20N, Warner
310 Instruments Corp.), attached the holder to the V_m probe of an OC-725 two-electrode Oocyte Clamp
311 (Warner Instruments Corp.), and mounted the probe on a model MM-33R micromanipulator
312 (Warner Instruments Corp.). The V_m microelectrodes had resistances of ~0.3 – ~0.6 MΩ.

313 The microelectrodes for measuring intracellular pH (pH_i) were identical to the V_m electrodes
314 except for the following fabrication process. In order to remove moisture, we placed the pulled
315 micropipettes, with tips upwards, into the cylindrical holes of a reusable aluminum block
316 (machined to create "legs" and thereby allow gases to circulate from beneath, and with smaller
317 concentric cylindrical holes extending the entire height of the block to allow access of gases from
318 below, to the interior of the glass capillary), placed the block into the bottom of a 100-mm Pyrex
319 petri dish, covered the electrodes and block with an inverted 250-mL beaker, placed the petri dish
320 on an open metal rack of an oven at 200 °C, and then baked overnight. With the microelectrodes
321 still in the 200 °C oven, we then silanized them by tilting the beaker slightly and depositing 80 μL
322 of *bis*-di-(methylamino)-dimethylsilane (Sigma-Aldrich, catalog #14755) between the legs of the
323 aluminum block, releasing the breaker, and allowing the silane fumes to interact with the
324 microelectrodes for 40 min before removing beaker. The silanized electrodes cured in the oven at
325 200 °C until ready for use. We used a hand-drawn, soft-glass pipette with a long tip to backfill
326 each pH_i electrode with a liquid pH-sensitive sensor (catalog #95293, Hydrogen Ionophore I,
327 mixture B, Fluka Chemical Corp., Ronkonkoma, NY), as described by (Ammann *et al.*, 1981),
328 creating a column that extended ~1 mm from the microelectrode tip. We then backfilled an
329 microelectrode with a buffer solution (containing, in mM, 40 KH_2PO_4, 23 NaOH, 15 NaCl,
330 adjusted to pH 7.0), inserted the electrode into a half-cell/microelectrode holder (model # ESW-

331 F20N, Warner Instruments Corporation), attached the holder to one probe of a model FD223 dual
332 high-impedance electrometer, World Precision Instruments [WPI], Inc., Sarasota, FL), and
333 mounted the probe on a model MM-33R micromanipulator (Warner Instruments Corp.). The pH_i
334 microelectrodes had resistances of ~0.3 – 0.6 MΩ.

335 After placing the tips of the V_m and pH_i microelectrodes in ND96 solution in the chamber
336 channel (which we now refer to as the "bath"), we obtained V_m by an analog electronic subtraction
337 of the system ground of the OC-725 amplifier from the signal of the V_m electrode. We similarly
338 obtained the voltage due to pH_i by electronically subtracting the signal of the V_m electrode from
339 the signal of the pH_i electrode. For a schematic representation of the configuration of the
340 electronics for obtaining V_m (this section) and the voltages due to pH_i (this section) and pH_S (next
341 section), see figure 7c in Musa-Aziz *et al.* (2010). The device that performed the subtractions (Yale
342 University Subtraction Amplifier, v3.1) also appropriately scaled the voltages for the inputs of an
343 analog-to-digital converter, installed in a Windows-based computer. With the tips of the V_m and
344 pH_i electrodes (and also the pH_S electrode, simultaneously; see next section) in the bath, we
345 obtained the slope of the pH_i electrodes as we used the aforementioned solution-delivery system
346 (see previous section) to flow a pH standard at pH 6.0 (catalog # SB104-1) continuously through
347 the chamber channel, recorded the voltage due to that pH, used the valve system to switch the
348 flowing solution to a second, pH-8.0 standard (catalog # SB112-20), and then recorded the
349 corresponding voltage. We typically switched between standards in a pH-6→8→6→8 sequence,
350 accepting pH_i microelectrodes that completed their electrical response—which also included the
351 time for the solution in the chamber channel to fully change composition—within ~5 s (~2 s for
352 pH_S electrodes) and had slopes in the range of 53 to 60 mV/pH unit. After the recordings in the
353 final pH-calibration solution, we re-introduced the ND96 solution into the bath, and then added
354 the oocyte to the chamber channel. After impaling the oocyte with the V_m electrode, and with the
355 tip of the pH_i electrode near the oocyte, we obtained a single-point pH calibration of the pH_i
356 microelectrode in the ND96 solution (defined as having a pH 7.50). We then impaled the oocyte
357 with the pH_i microelectrode. After stabilization, oocytes had spontaneous V_m values at least as
358 negative as –40 mV. We continuously recorded pH_i to judge the integrity of the oocyte and
359 compare the pH_i time course with that of surface pH. In the present paper, we are not presenting
360 the pH_i data, which nevertheless are similar to those of our previous studies (Musa-Aziz *et al.*,
361 2009*a*, 2010, 2014*a*, 2014*b*).

362 **Measurement of surface pH.** We measured surface pH with liquid-sensor pH
363 microelectrodes that we fabricated and employed in the same way as we did for pH_i
364 microelectrodes (see above), but with four differences. First, we pulled the pH_S microelectrodes
365 from standard-walled (rather than thin-walled) borosilicate microfilament glass tubing (Part No.
366 G200F-4, 2.0 mm OD ×1.16 mm ID, Warner Instruments). Second, we used a microforge to break
367 off and fire polish the tips (inner diameter ≅ 20 μm at tip) as one would for a giant-patch pipette
368 (Musa-Aziz *et al.*, 2010). It was to facilitate the fire polishing that we used the standard-walled
369 glass tubing. Third, we used a vented microelectrode holder (model # ESW-F20N, Warner
370 Instruments Corp.) mounted on a model MM-33L micromanipulator. The vent prevented pressure
371 buildup that would otherwise have pushed the liquid pH sensor out of the wide electrode tip as we
372 pushed the pH_S electrode into the holder. Note that we attached the microelectrode holder of the
373 pH_S electrode to the second of two inputs of the FD223 electrometer. And fourth, after obtaining
374 the pH_S-electrode slope (which we did at the same time as obtaining the pH_i electrode slope, as
375 described above) and single-point calibration of the pH_S electrode in ND96, we used an ultra-fine
376 computer-controlled micromanipulator (model MPC-200 system, Sutter Instrument Company) to
377 positioned the blunt tip of the pH_S electrode near the oocyte's equator (i.e., between the upward-
378 facing animal pole and downward-facing vegetal pole), and ~5 degrees behind the meridian (i.e.,
379 barely in the "shadow" of the flowing extracellular solution) until the pH_S electrode tip just touched
380 the surface of the oocyte (Musa-Aziz *et al.*, 2010, 2014*a*). We then further advanced the tip by ~40
381 μm to create a slight dimple in the membrane. Periodically during the experiment (indicated by
382 vertical gray bands in each panel of Figure 2*B*, Figure 3, and Figure 6), we withdrew the electrode
383 ~300 μm from the oocyte for recalibration in the bulk extracellular fluid (bECF) of the bath (i.e.,
384 pH 7.50).

385 The external reference electrode for the pH_S measurement was a calomel half-cell, bridged to
386 the chamber channel via a long glass micropipette filled with 3M KCl, connected to a model 750
387 electrometer (WPI), and positioned so that its tip was just downstream of the oocyte. We obtained
388 the pH_S signal by an analog electronic subtraction of the calomel signal from the signal of the pH_S
389 electrode.

390 We established a virtual ground with an Ag/AgCl half cell (connected to the I_{Sense} input of the
391 voltage-clamp amplifier) bridged to the chamber by a second glass microelectrode filled with 3M

392 KCl, and positioned the tip of this second bridging pipette close to that of the first, that is, just
393 downstream of the oocyte.

394 **Measurement of osmotic water permeability.** We measured P_f as described by (Zhang *et*
395 *al.*, 1990; Preston *et al.*, 1992, 1993). Using an approach similar to those in previous studies by
396 our group (Virkki *et al.*, 2001; Musa-Aziz *et al.*, 2009*a*), we dropped an oocyte into a Petri dish
397 containing a hypotonic solution (80 mOsm; Solution #6, Table 1) to induce cell swelling and, while
398 illuminating from beneath the dish, used a video camera to obtain images of the oocyte (1/s × 60
399 s). Using a small metal sphere next to the oocyte as a size reference, we determined the projection
400 areas of the oocyte, and—assuming the oocyte to be a perfect sphere—computed idealized oocyte
401 volume (V_{Oocyte}) and idealized oocyte surface area as a function of time. We estimated the actual
402 surface area (S, in cm^2) by multiplying the idealized surface area by a factor of 9 (Chandy *et al.*,
403 1997). We computed P_f from the following equation:

404
$$P_f = \underbrace{\frac{\left(\frac{dV_{Oocyte}}{dt}\right)_{max}}{S \times \Delta Osm \times V_W}}_{\text{units: } cm\,/\,s},$$

405 the form of which differs slightly from that of Zhang *et al.*, (1990).[4] Here, $(dV_{Oocyte}/dt)_{max}$ is the
406 maximum time rate of change of cell volume (i.e., the maximal H_2O influx, or $J_{V,max}$, in $cm^3\ s^{-1}$),
407 ΔOsm is the initial osmotic gradient across the oocyte membrane (i.e., 195 – 80 = 115 mOsm,
408 expressed as mol cm^{-3}), and V_w is the molar volume of water (18.1 $cm^3\ mol^{-1}$). As for the
409 electrophysiological studies, we performed all P_f assays at room temperature (~22 °C).

[4] To obtain P_f in the proper units (cm s^{-1}) in the above equation, the derivation by Zhang *et al.*, (1990) requires that the division of "moles of osmotically active particles" (in the ΔOsm term) by "moles of water" (in the V_W term) yield a numerical result that is unitless, which of course is impossible. This inconsistency arises during the derivation of the water-flux equation when one switches from describing the energy of water (i.e., RT) as "per mole of water" per se to the energy of water "per mole of osmotically active solute" during the introduction of the Van't Hoff equation. The introduction of a phantom conversion factor with a value of unity—but with the units "(per mole of osmotically active solute)/(per mole of water)"—eliminates the inconsistency.

410 ## Protocols for physiological experiments

411 Figure 1*A–J* illustrates the sequence of events in our experimental protocols.

412 **Electrophysiological assays.** On the day of an experiment, we followed a 10-step protocol:

413 (A) Use a transfer pipette to pick up an untreated oocyte from a well of a 6-well plate (each
414 well containing OR3 medium + ~30 oocytes, all injected with the same material) and drop the
415 oocyte into a petri dish containing ND96 (Solution #1, Table 1). After flushing the transfer pipette
416 tip several times with ND96 (to remove OR3).

417 (B) Use the transfer pipette to move the washed oocyte to an identified well of a 24-well plate
418 (1 oocyte/well) containing ND96. Repeat this procedure for several oocytes, each of which will
419 remain in its well (1–3 hours) until we …

420 (C) Use the transfer pipette to place the oocyte in the chamber, begin flowing ND96, and
421 measure V_m, pH_i, and pH_S under basal conditions.

422 (D) Monitor pH_S as we replace ND96 with either the 5% CO_2/33 mM HCO_3^- solution (Solution
423 #3, Table 1; as in Figure 2*B*, Figure 3) or the 0.5 mM NH_3/NH_4^+ solution (Solution #5, Table 1; as
424 in Figure 5*B*, Figure 6); all oocytes in the study underwent this control assay.

425 (E) Immediately upon completion of the pH_S assay, use a transfer pipette to return the oocyte
426 from the chamber to its original well and incubate the oocyte at ~22°C in ND96. We serially
427 process all oocytes from a 24-well plate up to this stage (i.e., steps 'C' through 'E') and then pause.
428 Thus, this second period of incubation in ND96 (step 'E') ranges from ~30 min to ~3 h.

429 (F) Use a transfer pipette to move each oocyte in the 24-well ND96 plate to a corresponding
430 well in one of three new 24-well plates. Here, the wells contain one of the following three
431 solutions: (F_1) 1 mM pCMBS dissolved in ND96 (Solution #7, Table 1) 30 min incubation; see
432 Figure 3*DEF*, Figure 6*DEF*, Figure 7, Figure 8, or Figure 9*CD*); (F_2) 100 μM DIDS dissolved in
433 ND96 (Solution #8, Table 1; 60 min incubation; see Figure 3*GHI* or Figure 6*GHI*); or (F_3) ND96
434 without an added drug ("sham").

435 (G) Wash the oocyte. Except in a few cases (see indented paragraph below), we wash the
436 oocyte ×3 in a petri dish containing ordinary ND96, as follows. We use a transfer pipette to pick
437 up an oocyte from a 24-plate (step 'F') and release the oocyte into a petri dish containing ND96,
438 quickly pick up and released the oocyte into this wash solution twice more (to remove excess drug,
439 if present). At this point, most oocytes progress immediately through step 'H' (below). However,

440 in a minority of experiments (see Figure 3*JKL*), we serially treated oocytes with both pCMBS and
441 DIDS. Here, oocytes previously treated with pCMBS (step 'F_1') we exposed to DIDS, as indicated
442 by steps $\alpha_1 \rightarrow \alpha_2 \rightarrow \alpha_3$. Conversely, oocytes previously treated with DIDS (step 'F_2') we exposed to
443 pCMBS, as indicated by steps $\beta_1 \rightarrow \beta_2 \rightarrow \beta_3$. In one experiment without any drugs, we also followed
444 the steps $\gamma_1 \rightarrow \gamma_2 \rightarrow \gamma_3$ ("double sham").

445 Not illustrated in Figure 1 is a protocol variant that we employ in a few cases (i.e.,
446 Figure 9*AB/right bars*) in which we introduce an additional step between 'F_2' and 'G'.
447 Here, after treating an oocyte with DIDS (step 'F_2'), we scavenge unreacted DIDS with
448 albumin as follows. After using a transfer pipette to pick up the oocyte from the DIDS-
449 containing ND96 solution, we release the oocyte into a petri dish containing 0.2%
450 albumin in otherwise DIDS-free ND96 (Solution #9, Table 1), and allow the oocyte to
451 remain in the albumin solution for 20 min. We then wash off the albumin in step 'G' by
452 transferring the oocyte to a petri dish containing ordinary ND96, and pick up and release
453 the oocyte ×3 using a transfer pipette.

454 (H) Use a transfer pipette to move the oocyte from the petri dish (step 'G') to an identified well
455 in one of three new 24-well plates, all containing ND96, in preparation for the next assay.

456 (I) Transfer the oocyte back to the chamber and (as in step 'C'), and again measure the new
457 basal V_m, pH_i, and pH_S.

458 (J) Monitor (as in step 'D'), for the second time, the pH_S transient as we replace ND96 with
459 the CO_2/HCO_3^- (or NH_3/NH_4^+) solution.

460 Thus, oocytes in the top row of Figure 3 (i.e., Figure 3*ADGJ*) went through one of the following
461 two sequences: Panels *A*→*D* or *A*→*J*, which requires 12–18 h for an entire group of 24 oocytes in
462 a day's work. Not all oocytes survived the entire protocol (as judged by the color/integrity of the
463 animal pole).

464 ***P_f* assays.** On the same day that we performed our pH_S assays, we also performed P_f assays
465 on separate cells from the same oocyte batch (i.e., oocytes prepared from the same ovary). On the
466 same day as pH_S experiments, we: (1) Use a transfer pipette to remove 6 untreated oocytes of each
467 experimental group—hAQP1, C189S mutant, or hAQP1 FLAG-tagged—from an identified 6-well
468 plate containing ND96 (i.e., a total of 18). (2) Place the oocytes—as quickly as possible—in a Petri
469 dish containing hypotonic ND96 (Solution #6, Table 1). (3) Use a video camera (described above)

470 to monitor cell swelling; oocytes of each group underwent this control assay. (4) Immediately
471 remove the oocytes from the hypotonic solution to identified wells in another Petri dish containing
472 standard ND96 solution to wash the oocytes ×3 at ~22°C (described above under
473 electrophysiological assays). (5) Incubate at ~22°C either for (5a) 30 min in ND96 containing 1
474 mM pCMBS (Solution #7, Table 1), or (5b) 1 hour in ND96 containing 100 μM DIDS (Solution
475 #8, Table 1). (6) Wash the oocytes (as described under electrophysiological assays, point '5a'). (7)
476 Transfer the oocytes to a Petri dish containing hypotonic, drug-free ND96 as in '2' above. (8)
477 Monitor swelling as in '3' above.

478 Generation of the DIDS antibody

479 **Generation of DIDS-fusion protein.** We used two rabbits to produce polyclonal antibodies
480 against DIDS, as described by Garcia & Lodish (1989). Briefly, we reacted 2.4 mM DIDS (catalog
481 # D3514, Sigma-Aldrich), with 5 mg keyhole limpet hemocyanin (KLH;, catalog # H7017, Sigma-
482 Aldrich) in 500 μL of phosphate buffer saline (PBS; i.e., 150 mM NaCl, 10 mM phosphate buffer,
483 pH 7.0) in the dark at 37°C × 40 min. Afterwards, we centrifuged the sample × 30 s in an Eppendorf
484 benchtop centrifuge (catalog # 5415C, TFS) to remove large insoluble aggregates After pooling
485 yellow supernatants from several centrifuge tubes, we dialyzed against PBS at 4°C overnight in a
486 slide-a-lyzer dialysis cassette (TFS). The following day, we removed the KLH-DIDS sample from
487 the cassette; quantified the DIDS by absorbance spectroscopy at 340 nm, assuming a molar
488 extinction coefficient (ε) of 54,000 M^{-1} cm^{-1}; aliquoted the dialyzed KLH-DIDS solution; and
489 immediately used it for immunization.

490 For both rabbits, we separately processed each of three blood samples (see above)—2 lots of
491 ~30–50 mL plus the terminal sample. We centrifuged the blood for 10 min at 1000 ×g using an
492 Eppendorf bench top centrifuge to isolate the serum, and then evaluated antigenicity on western
493 blots of DIDS-labeled AQP1. We purified the antibodies (mainly IgG) from the remainder of the
494 serum using a Protein A column (Catalog # 20356, TFS), following the manufacturer's
495 instructions; estimated [IgG] by measuring absorbance at 280 nm (assuming ε = 210,000 $M^{-1}cm^{-}$
496 ^{1}) using a NanoDrop 2000c spectrophotometer (TFS); separated the material into aliquots
497 corresponding to 1 mg/mL of anti-DIDS antibody; and stored the aliquots at either –20°C for short-
498 term storage or –80°C for long-term storage.

499 ## Biochemical experiments

500 **Isolation of oocyte membranes.** We used a previously described method (Leduc-Nadeau *et*
501 *al.*, 2007), except that, after disrupting oocytes and centrifuging, we removed the supernatant and
502 added fresh buffer to the pellet, repeating the procedure until the supernatant was clear (i.e., void
503 of yolk).

504 **Purification of oocyte membrane proteins.** We resuspended isolated oocyte membranes in
505 Tris-Buffered Saline (TBS, 50 mM Tris HCl, pH 7.4, 150 mM NaCl) + 2% n-dodecyl-β-D-
506 maltopyranoside (DDM; Sol-Grade, catalogue #D310S, Anatrace, Maumee, OH), incubated at
507 4°C × 2h, centrifuged at 16,000 × g at 4°C × 30 min, and then collected the supernatant containing
508 the solubilized membrane proteins and diluted it so that [DDM] was ≤ 0.5%.

509 **Overexpression of AQP1-FLAG in *Pichia pastoris*.** We ligated N-terminally FLAG-tagged
510 hAQP1 (MDYKDDDDKASEFKKKL… ; FLAG sequence underscored, hAQP1 sequence double
511 underscored) into the pPICZ-A vector (Invitrogen, Carlsbad, CA), induced protein expression with
512 methanol × 72 h at 26 ºC, harvested the yeast by centrifugation, and obtained spheroplasts using
513 zymolyase treatment (60 U/mL in 1 M sorbitol, 1 mM EDTA, 10 mM citrate buffer, pH 5.8) as
514 previously described (Gustin *et al.*, 1998). We then equally divided the spheroplasted cells into
515 two groups (i.e., no DIDS and added 100 µM DIDS), incubated × 1 h at ~22 °C, and then
516 solubilized overnight at 4°C in TBS + 2% DM, with cOmplete™ Protease Inhibitor Cocktail
517 (catalog #11697498001, Roche, Mannheim, Germany). Following membrane solubilization, we
518 clarified the material by low speed centrifugation, mixed with anti-FLAG resin (catalog #A2220,
519 Sigma-Aldrich), and eluted proteins from a column using TBS + 0.1% DM + 500 µg/mL FLAG
520 peptide (catalog #F4799, Sigma-Aldrich) at pH 7.4. In some cases, we subjected FLAG-purified
521 AQP1 to size-exclusion chromatography using a Sephadex 75 column.

522 **Western blotting of membrane proteins from oocytes or *Pichia pastoris*.** We separated
523 proteins extracted from oocyte membranes by SDS-PAG using Tris-Glycine 4–20% gels (BioRad
524 Laboratories, Hercules, CA) or proteins from extracted from *Pichia* membranes using 12% Tris-
525 Glycine gels; transferred the proteins to polyvinylidene difluoride (PVDF) membranes using an
526 iBlot 7-Minute Blotting System (TFS); and subsequently blocked the cross-linked proteins with
527 Tris-buffered saline with tween (TBST), comprising 25 mM Tris at pH 7.4, 150 mM NaCl, 0.05%
528 Tween-20 (catalog # P9416, Sigma-Aldrich) + 5% milk powder × 1 h.

529 We probed blots from oocyte samples with a polyclonal anti-AQP1 (catalog # AQP11-A,
530 Alpha Diagnostics, San Antonio, USA), and blots from *P. pastoris* samples with monoclonal anti-
531 FLAG (catalog # F3165-2MG, Sigma-Aldrich) or polyclonal anti-DIDS (made in-house, see
532 above), applying all primary antibodies at 1:1000 dilution from their stocks in TBST + 5% milk,
533 at 4°C overnight. The next day, we washed the blot ×5 with TBST × 10 min. We detected the
534 primary polyclonal antibodies (i.e., anti-AQP1 and anti-DIDS) with an HRP-conjugated goat anti-
535 rabbit secondary antibody (catalog # 1706515, BioRad Laboratories), and detected the primary
536 monoclonal antibody (i.e., anti-FLAG), an HRP-conjugated goat anti-mouse secondary antibody
537 (catalog # STAR207P, BioRad Laboratories). We applied both secondary antibodies at 1:5000
538 dilution from their stocks in TBST × 1 h, washed the blot ×5 with TBST × 10 min, developed the
539 immunoblots using ECL Prime Western Blotting Detection Reagent (catalog # 12316992, GE
540 Healthcare Amersham, Piscataway, NJ), acquired images with a Typhoon Trio gel-documentation
541 system (GE Healthcarefryan), and evaluate band density patterns using Image J software (NIH,
542 Bethesda, MD).

543 Statistics

544 We present data as the mean ± S.D. (standard deviation), and define N as the number of
545 different frogs used and n as the number of replicate experiments (i.e., oocytes) for each condition
546 in each dataset. We define *m* as the number of comparisons in each dataset. Statistical analyses are
547 performed using Origin 2024 software. Statistical comparisons among means were performed
548 using a one-way analysis of variance (ANOVA) among all groups, followed by Holm-Bonferroni
549 mean comparison (Holm, 1979) to control for type I errors across multiple comparisons,
550 establishing the familywise error rate (FWER) to $\alpha = 0.05$. In brief, the unadjusted *P*-values for all
551 *m* comparisons in each dataset from lowest to highest. In the first test, we compare the smallest
552 unadjusted *P*-value to the first adjusted α value, α/m. Upon rejection of the null hypothesis, we
553 compare the second-smallest *P*-value to the second adjusted α value, $\alpha/(m-1)$, and continue the
554 process accordingly. If the unadjusted *P*-value is ≥ the adjusted α at any stage, the null hypothesis
555 is accepted, rending all subsequent hypotheses in the test group null. We conducted one-sample t-
556 tests (α=0.05) to ascertain whether the channel-dependent $(\Delta pH_S^*)_{CO_2}$ was significantly different
557 from zero when oocytes were treated with both pCMBS and DIDS. If $P < 0.05$, the $(\Delta pH_S^*)_{CO_2}$
558 was considered significantly greater than zero. We conducted one-sample t-tests (α=0.05) to
559 ascertain whether the channel-dependent $(\Delta pH_S^*)_{NH_3}$, was significantly different from zero when

560 oocytes were treated with pCMBS. If $P < 0.05$, the $(\Delta pH_S^*)_{CO_2}$ was considered significantly greater
561 than zero.

562 # Results

563 ## Surface-pH Measurements for AQP1-WT and AQP1-C189S

564 **pH_S measurements for CO_2 transport.** Figure 2*A* is a schematic representation of the
565 reaction and diffusion events that take place as we switch the bath solution—that is, the bulk
566 extracellular fluid—from ND96 to another that contains 5% CO_2/33 mM HCO_3^- at a constant pH
567 of 7.50. This solution change not only leads to a net influx of CO_2 that lowers intracellular pH
568 (Roos & Boron, 1981) but also lowers CO_2 concentration near the outer surface of the cell
569 membrane ($[CO_2]_S$). This decrease in $[CO_2]_S$ has two effects. First, it creates a gradient for CO_2
570 diffusion from the bECF to the cell surface, which partially replenishes CO_2 at the cell surface but
571 by itself has no effect on pH. Second, it drives the reactions $HCO_3^- + H^+ \rightarrow H_2CO_3 \rightarrow CO_2 + H_2O$
572 at the cell surface, which also partially replenishes CO_2. This reaction causes an alkaline pH_S
573 transient, the maximal excursion of which we define as ΔpH_S (Endeward *et al.*, 2006; Musa-Aziz
574 *et al.*, 2009*a*; Geyer *et al.*, 2013). Our colleagues have used 3D reaction-diffusion models to
575 simulate these pH_S and pH_i changes as CO_2 diffuses into a spherical cell (Somersalo *et al.*, 2012;
576 Musa-Aziz *et al.*, 2014*a*, 2014*b*; Occhipinti *et al.*, 2014; Calvetti *et al.*, 2020).

577 Figure 2*B* shows a representative pH_S recording from a H_2O-injected or "control" oocyte
578 during such a solution change (for solution composition, see Table 1). The vertical gray bands in
579 the figure indicate periods during which we withdraw the tip of the extracellular pH microelectrode
580 from its previous position, in which its tip created a small dimple (~40 μm) in the oocyte surface,
581 to a distance of ~300 μm for recalibration in the bECF, which we assume to have a pH of precisely
582 7.50. We describe the recalibration in the legend of Figure 2.

583 Figure 2*C* shows a representative western blot of membrane preparations (see Methods) of
584 oocytes injected with H_2O or cRNA encoding either AQP1-WT or AQP1-C189S. The lower
585 band(s) at ~25 kDa presumably represents unglycosylated or core-glycosylated AQP1 in the
586 endoplasmic reticulum. The upper bands at ~37 kDa represent mature-glycosylated AQP1, much
587 of which is presumably at the plasma membrane. Assuming that the AQP1 antibody has similar
588 sensitivities for the WT and C189S proteins, we conclude that *Xenopus laevis* oocytes express
589 similar amounts of each.

590 Figure 3 shows a series of 12 representative pH_S recordings, the first of which, in Figure 3*A*,
591 is a replicate of Figure 2*B*. We can see that the ΔpH_S induced by the CO_2 influx in this H_2O-

592 injected control oocyte is much smaller (upward orange arrow in Figure 3*A*) than in a day-matched
593 oocyte injected with cRNA encoding hAQP1-WT (upward green arrow in Figure 3*B*).

594 We define $(\Delta pH_S^*)_{CO_2}$ as the difference between the CO_2-induced ΔpH_S value of an oocyte
595 expressing a channel protein (upward black arrow in inset of Figure 3*B*) and the mean ΔpH_S for
596 all day-matched control oocytes (e.g., Figure 3*A*). This difference is a semiquantitative index of
597 the channel-specific CO_2 flux (Musa-Aziz *et al.*, 2009*a*; Somersalo *et al.*, 2012; Calvetti *et al.*,
598 2020). The leftmost bar in Figure 4*A* represents the mean $(\Delta pH_S^*)_{CO_2}$ value for 34 oocytes
599 expressing AQP1-WT in the absence of inhibitors.

600 To assess the importance of the monomeric pore, we examined the effect of pCMBS, which,
601 like $HgCl_2$, covalently modifies Cys-189 near the extracellular entrance of the monomeric pore
602 and reduces the component of P_f due to AQP1 (Preston *et al.*, 1993), which we define as P_f*.
603 Preston et al showed that $HgCl_2$ has no effect on P_f if oocytes express the C189S mutant of AQP1
604 (Preston *et al.*, 1993). On the basis of pH_i measurements, Cooper and Boron (1998) showed that
605 pCMBS significantly reduces the CO_2 permeability of oocytes expressing AQP1-WT, but that this
606 effect is absent oocytes expressing AQP1-C189S. In the present study, in which we now monitor
607 pH_S, experiments on individual oocytes confirm that pretreatment with 1 mM pCMBS (see
608 Methods) reduces the CO_2-induced ΔpH_S in an AQP1-WT oocyte (Figure 3*E* vs. *B*) but not in an
609 oocyte expressing AQP1-C189S (Figure 3*F* vs. *C*). pCMBS has no effect on a H_2O-injected oocyte
610 (Figure 3*D* vs. *A*), for which ΔpH_S is already small. We conclude that pCMBS reduces but does
611 not eliminate the ΔpH_S due to AQP1 (Figure 3*E* vs. *D*).

612 The leftmost bar in Figure 4*B* represents the mean $(\Delta pH_S^*)_{CO_2}$ from 22 oocytes expressing
613 AQP1-C189S in the absence of inhibitors. This $(\Delta pH_S^*)_{CO_2}$ value is very similar to that for oocytes
614 expressing AQP1-WT (leftmost bar in Figure 4*A*). A comparison of the first and second bars in
615 Figure 4*A* and *B* shows that pCMBS reduces $(\Delta pH_S^*)_{CO_2}$ by somewhat more than half in oocytes
616 expressing AQP1-WT, but has no significant effect in AQP1-C189S oocytes. These data support
617 the hypothesis that, of the CO_2 that transits AQP1, a major component moves through the same
618 monomeric pores as H_2O.

619 While studying HCO_3^- transport, Forster et al unexpectedly found that DIDS blocks a large
620 fraction of CO_2 permeability of human RBCs (Forster *et al.*, 1998). Endeward et al found that, in
621 RBCs genetically deficient in AQP1, DIDS has a reduced effect on CO_2 permeability (Endeward
622 *et al.*, 2006). Here, in the present experiments on single oocytes, we find that pretreatment with

623 100 μM DIDS reduces the CO_2-induced ΔpH_S in both an AQP1-WT oocyte (Figure 3*H* vs. *B*) and
624 an AQP1-C189S oocyte (Figure 3*I* vs. *C*), but not in a H_2O-injected oocyte (Figure 3*G* vs. *A*), for
625 which ΔpH_S is already small.

626 The third bars in Figure 4*A* and *B* summarize mean $(\Delta pH_S^*)_{CO_2}$ values from a larger group of
627 oocytes pretreated with DIDS. A comparison of the first and third bars shows that DIDS reduces
628 $(\Delta pH_S^*)_{CO_2}$ by more than half in oocytes expressing either AQP1-WT (Figure 4*A*) or AQP1-C189S
629 (Figure 4*B*). These data are consistent with the hypothesis that a significant fraction of CO_2 moves
630 through AQP1 by a DIDS-sensitive pathway that is unaffected by the C189S mutation in the
631 extracellular mouth of the monomeric pore.

632 Returning to experiments on individual oocytes, we see that the sequential exposure of an
633 AQP1-WT oocyte to pCMBS and then DIDS substantially reduces the CO_2-induced ΔpH_S (Figure
634 3*K* vs. *B*). Moreover, and the size of the ΔpH_S for the pCMBS/DIDS-treated AQP1-WT oocyte
635 (Figure 3*K*) is about the same as for H_2O-injected oocytes ±inhibitors (Figure 3*A,D,G,J*). In an
636 AQP1-C189S oocyte, the combination of pretreating with pCMBS then DIDS reduces the CO_2-
637 induced ΔpH_S (Figure 3*L* vs. *C*), but by no more than DIDS alone (Figure 3*I* vs. *C*).

638 The fourth bars in Figure 4*A* and *B* summarize mean $(\Delta pH_S^*)_{CO_2}$ values from a larger group of
639 oocytes, in experiments in which we treated with pCMBS and DIDS in either order. A comparison
640 of the first and fourth bars shows that pCMBS+DIDS reduces $(\Delta pH_S^*)_{CO_2}$ by slightly more than
641 100% in AQP1-WT oocytes (Figure 4*A*). In the AQP1-C189S oocytes, pCMBS+DIDS reduces
642 $(\Delta pH_S^*)_{CO_2}$ to about the same extent as DIDS alone (Figure 4*B*), about 40%. Taken together, the
643 data in Figure 3 and Figure 4*A* and *B* are consistent with the hypothesis that, in addition to the
644 component of CO_2 that moves through the four monomeric pores, another component—at least as
645 large—moves through an entirely separate, DIDS-sensitive pathway.

646 Figure 4*C* summarizes the results of ND96 sham experiments in which—in step F_3 of Figure
647 1—we simulated either a 30-min pCMBS exposure (n = 3) or a 60-min DIDS exposure (n = 2).
648 The averages of the two sham groups were nearly identical to that of the control group, showing
649 that the oocytes can tolerate these long protocols.

650 **pH_S measurements for NH_3 transport.** Figure 5*A* is a schematic representation of the reaction
651 and diffusion events that take place as we exposing an oocyte to a solution containing 0.5 mM
652 NH_3/NH_4^+. Here, the changes in pH_S are opposite in direction to those caused by CO_2/HCO_3^-

653 exposure. As the weak base NH_3 enters the cell, it causes a decrease in $[NH_3]_S$, which has two
654 effects. First, it provides a gradient for NH_3 diffusion from the bECF to the cell surface. By itself,
655 this diffusion, which partially replenishes NH_3 at the cell surface, has no effect on pH. Second, the
656 decrease in $[NH_3]_S$ also drives the reaction $NH_4^+ \rightarrow NH_3 + H^+$ at the cell surface, which also
657 partially replenishes NH_3. This reaction produces an acidic pH_S transient (Musa-Aziz *et al.*, 2009*b*,
658 2009*a*), so that $\Delta pH_S < 0$. Figure 5*B* shows a representative pH_S recording as we introduce
659 NH_3/NH_4^+.

660 Figure 6 shows a series of 9 representative pH_S recordings on individual oocytes, the first of
661 which, in Figure 6*A*, is a replicate of Figure 5*B*. We find that the NH_3-induced '$-\Delta pH_S$' is much
662 smaller in the H_2O-injected oocyte (Figure 6*A*) than in a day-matched oocyte expressing AQP1-
663 WT (Figure 6*B*). Subtracting the ΔpH_S from the H_2O-injected oocyte from the ΔpH_S from the
664 AQP1-WT oocyte yields the channel-dependent, NH_3-induced ΔpH_S—$(\Delta pH_S^*)_{NH_3}$ (Musa-Aziz *et*
665 *al.*, 2009*a*). The leftmost bar in Figure 7*A* represents the mean $(\Delta pH_S^*)_{NH_3}$ for 18 oocytes
666 expressing AQP1-WT in the absence of inhibitors.

667 In experiments on representative oocytes, we find that pretreating an AQP1-WT oocyte with
668 1 mM pCMBS markedly reduces '$-\Delta pH_S$' (Figure 6*E* vs. *B*), but has no effect in an AQP1-C189S
669 oocyte, where '$-\Delta pH_S$' remains high (Figure 6*F* vs. *C*); or in a H_2O oocyte, where '$-\Delta pH_S$' remains
670 low (Figure 6*D* vs. *A*). The leftmost bar in Figure 7*B* represents the mean $(\Delta pH_S^*)_{NH_3}$ value from
671 11 oocytes expressing AQP1-C189S in the absence of inhibitors. This $(\Delta pH_S^*)_{NH_3}$ value is
672 virtually identical to that for oocytes expressing AQP1-WT (leftmost bar in Figure 7*A*). A
673 comparison of first and second bars shows that pCMBS reduces '$-(\Delta pH_S^*)_{NH_3}$' by virtually 100%
674 in oocytes expressing AQP1-WT (Figure 7*A*), but has no effect in AQP1-C189S oocytes (Figure
675 7*B*).

676 Returning to experiments on individual oocytes, we see that DIDS has no effect on '$-\Delta pH_S$'
677 in a H_2O-injected control oocyte (Figure 6*G* vs. *A*), where '$-\Delta pH_S$' remains low; or in an AQP1-
678 WT oocyte (Figure 6*H* vs. *B*) or an AQP1-C189S oocyte (Figure 6*I* vs. *C*), where '$-\Delta pH_S$' remains
679 high. The third bars in Figure 7*A* and *B* summarize mean $(\Delta pH_S^*)_{NH_3}$ values from larger groups of
680 DIDS-pretreated oocytes. A comparison of the first and third bars in each panel shows that DIDS
681 is without effect on $(\Delta pH_S^*)_{NH_3}$ in oocytes expressing AQP1-WT (Figure 7*A*) or AQP1-C189S
682 (Figure 7*B*). Taken together, the data in Figure 6 and Figure 7 indicate that all of the NH_3 transiting
683 AQP1 moves via the same pathway as H_2O and one of the two major components of CO_2—namely

684 the four pCMBS-sensitive monomeric pores. None of the NH_3 moves via the alternate, DIDS-
685 sensitive pathway taken by the other major component of CO_2.

686 **Cell-swelling experiments.** In parallel with the CO_2 and NH_3 assays (Figure 4 and Figure 7),
687 we determined P_f*. In Figure 8*A*, we summarize our AQP1-WT data, which confirm earlier work
688 that shows that, in oocytes expressing AQP1-WT, mercurials reduce P_f* by about half (Macey,
689 1984; Preston *et al.*, 1993; Zeidel *et al.*, 1994; Musa-Aziz *et al.*, 2009*a*; Kabutomori *et al.*, 2018)
690 but that DIDS is without effect (Macey, 1984; Endeward *et al.*, 2006). Figure 8*B* confirms that the
691 AQP1-C189S mutation renders P_f* insensitive to pCMBS (Preston *et al.*, 1993; Cooper & Boron,
692 1998; Kabutomori *et al.*, 2018), and also shows that the mutation does not affect the lack of DIDS
693 sensitivity.

694 Modification of hAQP1 by DIDS

695 Via rapid and reversible electrostatic interactions, the two sulfonate groups of DIDS can
696 reversibly interact with cationic sites on proteins. Via slower covalent reactions with the $–NH_2$
697 group of lysine or –OH/–SH groups of other amino acids, the two isothiocyanate groups of DIDS
698 can act as a homobifunctional crosslinking reagent (Cabantchik & Rothstein, 1972; Lepke *et al.*,
699 1976).

700 **pH_S experiments on oocytes.** To assess whether the DIDS inhibition occurs via an
701 electrostatic or covalent interaction, we followed a DIDS exposure with an albumin wash (see
702 Methods) to scavenge non-covalently-bound DIDS. Figure 9*A* shows that the albumin wash does
703 not significantly reduce the degree to which the DIDS pretreatment reduces decreases $(\Delta pH_S^*)_{CO_2}$.
704 Because the inhibition is irreversible, the interaction of the DIDS with hAQP1 is most likely
705 covalent. To investigate this covalent modification, we performed the biochemistry experiments
706 (presented in next section) in which we FLAG-tagged hAQP1 at its N-terminus, overexpressed the
707 construct in *Pichia pastoris,* and prepared spheroplasts. Here, in control oocyte experiments, we
708 observe that the FLAG tag has no effect on the $(\Delta pH_S^*)_{CO_2}$ ±DIDS or ±albumin (Figure 9*B* vs. *A*).
709 We also find that the FLAG tag is without effect in P_f assays, ±pCMBS or ±DIDS (Figure 9*D* vs.
710 *C*).

711 **Biochemistry experiments.** In separate studies, as mentioned in the previous paragraph, we
712 overexpressed FLAG-tagged hAQP1 in *Pichia pastoris*, and prepared spheroplasts. We treated
713 intact spheroplasts with DIDS (or, as shams, without DIDS), solubilized the membranes in

714 detergent, and purified hAQP1 using an anti-FLAG resin. Further purification by size-exclusion
715 chromatography (Figure 10*A*) shows that DIDS treatment promotes the formation of higher–
716 molecular-weight hAQP1 species, as indicated by the increased peak height of the void volume
717 (V_0). We then pooled and concentrated fractions from each peak. Optical spectroscopy of this
718 material (Figure 10*B*) reveals the expected increase in absorbance centered at ~340 nm (brown
719 arrow; see Kodippili *et al.*, 2009), due to DIDS in the DIDS-treated vs. sham samples. We also
720 separated the pooled/concentrated material by SDS-PAGE, and transferred to membranes for
721 western blotting. In the anti-FLAG blot (Figure 10*C*), the dominant species are hAQP1 monomers
722 (≤50 kDa, arrows a–c) that, as we will see, represent mainly intracellular protein (i.e., not on
723 plasma membrane). Presumed dimers (arrow d) and tetramers (arrow e) are visible only in DIDS-
724 treated samples (lanes 2, 4, 6), and represent proteins accessible to DIDS at the outer cell surface.
725 In the anti-DIDS blot (Figure 10*D*), the monomeric species (dominant in the anti-FLAG blot) are
726 relatively poorly represented, whereas the presumed dimers and tetramers are clearly visible,
727 though only for DIDS-treated samples (lanes 2, 4, 6). These data are consistent with the hypothesis
728 that, once the divalent DIDS molecule reacts with one AQP1 monomer, the odds are high that the
729 DIDS crosslinks to one more to yield dimers and tetramers. Although we attempted to use mass
730 spectrometry to identify AQP1 residue(s) derivatized by DIDS, we were unable to achieve
731 coverage of protein fragments containing predicted DIDS-reactive sites near hydrophobic
732 transmembrane segments.

733 # Discussion

734 ## Pathways for NH_3 vs. CO_2

735 **NH_3 permeation through monomeric pores.** Although previous work had shown that AQP1
736 can serve as a conduit for NH_3 (Nakhoul *et al.*, 2001), the present work is the first direct
737 demonstration that the four monomeric pores of AQP1—which are responsible, of course, for all
738 H_2O conductance (Preston *et al.*, 1993)—are, in fact, also responsible for all NH_3 conductance.
739 This result is not unexpected, given the hydrophilicity of the monomeric pore (Walz *et al.*, 1997;
740 Sui *et al.*, 2001; Tajkhorshid *et al.*, 2002), and the similarities of the electronic structures of the
741 NH_3 molecule (i.e., 1 lone pair of electrons + 3 N–H bonds among 4 sp^3 hybrid orbitals) and the
742 H_2O molecule (i.e., 2 lone pairs + 2 O–H bonds among 4 sp^3 hybrid orbitals). The primary evidence
743 for our conclusion is that pCMBS reduces $(\Delta pH_S^*)_{NH_3}$ to zero (Figure 7*A*, center vs. left bars), an
744 effect abrogated by the C189S mutation (Figure 7*B*, analogous bars). On the other hand, none of
745 the NH_3 moves via the parallel DIDS-sensitive pathway, inasmuch as DIDS has no effect on
746 $(\Delta pH_S^*)_{NH_3}$ (Figure 7*A* and *B*, right vs. left bars). These results for NH_3 permeability parallel those
747 for osmotic water permeability in Figure 8.

748 **CO_2 permeation through monomeric pores.** The present work confirms earlier observations
749 (Cooper & Boron, 1998) that at least some CO_2 moves through AQP1 via the monomeric pores
750 and, furthermore, shows that this pathway amounts to about half the total $(\Delta pH_S^*)_{CO_2}$ signal. This
751 result is not unexpected, given the amphiphilic nature of CO_2. Moreover, the molecular dynamics
752 simulations of Wang *et al.* (2007) suggest that 40% of the CO_2 permeability of AQP1 is due to the
753 4 monomeric pores (i.e., ~10% per monomeric pore). Supporting evidence for this conclusion in
754 the present study is that pCMBS reduces $(\Delta pH_S^*)_{CO_2}$ by somewhat more than half (Figure 4*A*,
755 second bar from left vs. leftmost bar), an effect abrogated by the C189S mutation (Figure 4*B*,
756 analogous bars).

757 **CO_2 permeation through a parallel pathway.** The present work provides the first
758 physiological evidence for a second pathway for CO_2 through any AQP tetramer. This alternative
759 pathway is apparently parallel to the four monomeric pores. The primary evidence is that (a) DIDS
760 reduces $(\Delta pH_S^*)_{CO_2}$ by somewhat more than half in hAQP1-WT (Figure 4*A*, third bar from the left
761 vs. leftmost bar), (b) the C189S mutation does not affect the DIDS blockade (Figure 4*B*, analogous
762 bars), and (c) the combination of pCMBS and DIDS reduces $(\Delta pH_S^*)_{CO_2}$ to zero for oocytes

763 expressing AQP1-WT (Figure 4*A*, rightmost vs. leftmost bars), but still somewhat more than half
764 for oocytes expressing AQP1-C189S (Figure 4*B*, analogous bars).

765 Effect of Inhibitors

766 **DIDS.** Because the DIDS blockade is irreversible with both hAQP1-WT (Figure 9*A*) and
767 hAQP1-FLAG (Figure 9*B*), DIDS probably interacts covalently with nearly all functional AQP1
768 tetramers on the oocyte surface. Indeed, with DIDS-treated cells, western blots probed with a DIDS
769 antibody (Figure 10*D*) reveal presumed dimers and tetramers, but virtually no glycosylated
770 monomers (compare Figure 10*C* vs. *D,* blue arrows). Thus, we conclude that one or more bivalent
771 DIDS molecules likely crosslinks two or more monomers of almost all AQP1 tetramers on the cell
772 surface. These observations are consistent with the hypothesis that this crosslinking (observed in
773 biochemical experiments) is essential for blockade (observed in physiological experiments).
774 molecular dynamics simulations of Wang *et al.* (2007) suggest that ~60% of the CO_2 flux through
775 AQP1 occurs via the hydrophobic central pore that is largely devoid of H_2O because it is lined by
776 the sidechains of the following residues (from extracellular to intracellular sides): Val-50, Leu-54,
777 and Leu-58 (contributed by TM2), and Leu-174 and Leu-170 (from TM5). The mobility of a gas
778 like CO_2 through such a near vacuum is ~10^4 higher than in liquid water (see (Boron, 2010;
779 Rumble, 2022). Thus, even though central pores may comprise only a small fraction of total
780 membrane surface area, it is possible that such pores—on the background of a membrane with a
781 low intrinsic CO_2 permeability in the absence of AQP1 (Boron *et al.*, 2011)—could make a
782 significant contribution to overall CO_2 permeability. We propose that the central pore is the
783 anatomic substrate of the DIDS-sensitive component of CO_2 permeability of hAQP1-WT.

784 **Summing the effects of pCMBS and DIDS.** The mathematical simulations of Somersalo *et*
785 *al.* (2012) suggest that—in the region in which $(\Delta pH_S^*)_{CO_2}$ is most sensitive to the membrane
786 permeability to CO_2 (P_{M,CO_2})—$(\Delta pH_S^*)_{CO_2}$ should rise linearly with $\log(\Delta pH_S^*)_{CO_2}$ (see their figure
787 7b). If we assume that pCMBS and DIDS each decrease $(\Delta pH_S^*)_{CO_2}$ by 50%, then each drug must
788 produce a far greater fractional decrease in P_{M,CO_2}. Following the logic of the mathematical
789 simulations, the blockade of the monomeric pore by pCMBS should be accompanied by some
790 degree of blockade of the parallel CO_2 pathway (e.g., central pore). However, the converse is
791 apparently not true. That is, the blockade of the parallel pathway by DIDS seems not to produce
792 significant effects on the four monomeric pores inasmuch as DIDS has no effect on either
793 $(\Delta pH_S^*)_{NH_3}$ (Figure 7) or P_f^* (Figure 8). Such an overlapping effect of pCMBS on the monomeric

794 and parallel pathways is not unreasonable inasmuch as the target of pCMBS (i.e., C189) is near
795 the outward-facing NPA motif and the selectivity filter of the monomeric pore, both of which are
796 in close proximity to TM2, which lines the extracellular half of the central pore. We propose that
797 (1) pCMBS blocks CO_2 and NH_3 traffic through the monomeric pore and part of the CO_2 traffic
798 through the parallel pathway, and (2) DIDS blocks (most) CO_2 traffic through the parallel pathway
799 but no traffic through the monomeric pores.

800 Molecular Basis of Gas Selectivity

801 An important unresolved issue is the molecular basis for gas selectivity by AQPs (Musa-Aziz
802 *et al.*, 2009*a*; Geyer *et al.*, 2013).

803 **CO_2.** The present study indicates that the amphiphilic CO_2 molecule transits AQP1 via 2
804 pathways, the four hydrophilic monomeric pores and a parallel pathway (e.g., hydrophobic central
805 pore).

806 **NH_3.** Here we show that all NH_3 transits the four hydrophilic monomeric pores of AQP1; that
807 is, none moves via the parallel pathway (e.g., hydrophobic central pore). Considering the broader
808 family of AQPs, we predict that the hydrophobic parallel pathways (e.g., central pores) are never
809 important routes of NH_3 conductance, but rather that the characteristics of the monomeric pores
810 determine whether a particular AQP has a relatively high permeability to NH_3 (AQPs 3, 6, 7, 8,
811 9), or a relatively low NH_3 permeability (AQPs 2, 4, 5).

812 We suggest that, for the AQPs known to be permeable to CO_2 (AQPs 0, 4, 5, 6, 9), CO_2 transits
813 some combination of monomeric pores and a parallel, more hydrophobic pathway. For the AQPs
814 with limited CO_2 conductance (AQPs 2, 3, 7, 8), both the monomeric pores and the parallel
815 pathways presumably have less favorable physico-chemical characteristics. Because more-
816 hydrophobic molecules like O_2 and N_2 are less likely to transit through the monomeric pores, their
817 permeabilities through AQPs likely depend exclusively on the physico-chemical characteristics of
818 the parallel, hydrophobic pathway. Thus, the gas-selectivity profile of each AQP likely depends
819 on the physico-chemical nature of each gas and the unique set of physico-chemical properties of
820 the (at least 2) potential pathways through the tetramer.

Concluding Remarks

Our work establishes the proof of principle for blocking two pathways for CO_2, at least somewhat independently. Elimination of the monomeric pathway, combined with judicious mutations to the hydrophobic alternate pathway, could enable the design of channels with exquisite selectivity among gases. Such designer channels could improve industrial gas handling on a micro- or nanoscale, provide a simple approach for venting metabolically produced CO_2 in diving or space flight, provide control of CO_2 and N_2 conduction in agriculture, and enable precise O_2 control for medical therapies, synthetic biology, and life-support systems in underwater or space environments.

Additional information

Competing interests

All authors declare no conflict of interests.

Authors' contributions

R.M-A. contributed to the conception and design of the research; performed oocyte experiments; analyzed and interpreted the oocyte data; prepared figures; drafted and edited the manuscript. R.R.G. contributed to the conception and design of the research related to oocyte P_f experiments as well as *Pichia pastoris* research; performed all the *Pichia pastoris* experiments; analyzed and interpreted all results collected with *Pichia pastoris*; prepared figures; and drafted the manuscript. S-K. L. validated the cDNA clones for hAQP1 used in the experiments and contributed to the interpretation of pH_S experiments. F.J.M. contributed to the design of the research; prepared the figures; analyzed the statistics and interpreted results; drafted and edited the manuscript. W.F.B contributed to the conception and design of the research, and also edited the manuscript.

All authors approved the final version of the manuscript and all qualify for authorship, and all those who qualify for authorship are listed.

Funding

R.M.A. was supported for parts of this project by Fundação de Amparo a Pesquisa do Estado de São Paulo (FAPESP # 13/11364-3 and 18/22855-1). R.R.G. was supported by postdoctoral fellowship N00014-09-1-0246 from the Office of Naval Research and also by Fundação de Amparo a Pesquisa do Estado de São Paulo (FAPESP # 2013/10780). This work was also supported by National Institutes of Health Grants NS 18400, DK 8156, HL 160857 and U54 GM087519, as well as Office of Naval Research (ONR) Grants N00014-05-1-0345, N00014-08-1-0532, N00014-11-1-0889, N00014-14-1-0716, N00014-15-1-2060 and a Multidisciplinary University Research Initiative (MURI) grant N00014-16-1-2535 from the DoD (to W.F.B.).

Acknowledgements

We thank Duncan Wong for helpful discussions and computer support; Dale Huffman for engineering assistance and helpful discussions. We thank Steven Torontali for designing and

858 fabricating the oocyte chamber; Gerald Babcock for technical assistance and laboratory
859 management; Morley Schwebel; Charleen Bertolini, Rosalyn Forster, and Lesa Goodman for
860 administrative support. W. F. Boron gratefully acknowledges the support of the Myers/Scarpa
861 endowed chair. R. Musa-Aziz gratefully acknowledges Dr. Mark D. Parker (University at Buffalo:
862 State University of New York) for encouragement and helpful discussions, and gives special
863 thanks in memory of Dr. Gerhard Malnic (University of São Paulo, SP, BR) for his unwavering
864 support and advice.

Supporting information

N/A

Data Availability Statement

The data that support the findings of this study are available from the corresponding author upon reasonable request.

Footnotes

[1] We code-named the rabbits, and the antisera they produced, "Ren" and "Stimpy."

[2] In some later experiments, we instead put the oocytes and Ca^{2+}-free solution into 50-mL Falcon tubes (catalog # 14-959-49A, TFS) and agitated them using a Tube Rotator (Scientific Equipment Products, Baltimore, MD).

[3] We apparatus had this dual-solution arrangement to enable the use of out-of-equilibrium CO_2/HCO_3^- solutions in experiments that are not part of the present study.

[4] To obtain P_f in the proper units (cm s^{-1}) in the above equation, the derivation by Zhang *et al.*, (1990) requires that the division of "moles of osmotically active particles" (in the ΔOsm term) by "moles of water" (in the V_W term) yield a numerical result that is unitless, which of course is impossible. This inconsistency arises during the derivation of the water-flux equation when one switches from describing the energy of water (i.e., RT) as "per mole of water" per se to the energy of water "per mole of osmotically active solute" during the introduction of the Van't Hoff equation. The introduction of a phantom conversion factor with a value of unity—but with the units "(per mole of osmotically active solute)/(per mole of water)"—eliminates the inconsistency.

Figure legends

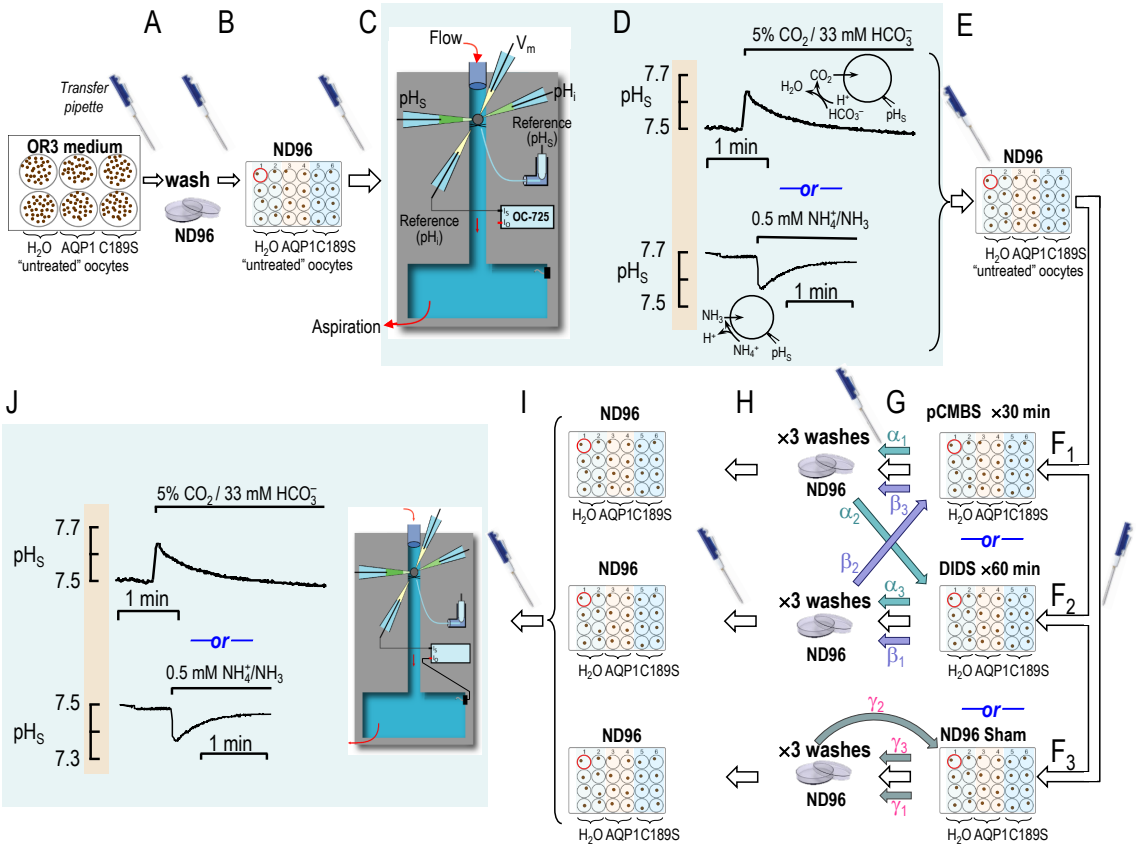

Figure 1: Flow chart showing experimental protocols. The letters "A", "B", "C" and so on are above broad arrows and near icons of a pipetter that identify the transfer of an oocyte (using a transfer pipette) from one step in our protocol to another. "D" and "J" are the initial and final electrophysiological recordings, respectively. The oocytes may be controls (injected with H_2O) or those expressing either hAQP1-WT (AQP1) or hAQP1-C189S (C189S). In transfer "F", we move the oocyte to a solution containing pCMBS (F_1), DIDS pCMBS (F_2), or no drug (F_3). As indicated by the white arrows, we can directly transfer from F_1 (or F_2 or F_3) to G to H. Alternatively, at transfer "F", we can execute subsidiary protocols (α/teal arrows, β/lavender arrows, γ/gray arrows) in which we return oocytes from washes in ND96 back to a solution containing an inhibitor (i.e., pCMBS or DIDS) or ND96 (i.e., sham drug exposure). Thus, an oocyte might undergo the teal-colored pCMBS/DIDS sequence ($\alpha_1 \rightarrow \alpha_2 \rightarrow \alpha_3$), the lavender-colored DIDS/pCMBS sequence ($\beta_1 \rightarrow \beta_2 \rightarrow \beta_3$), or the gray-colored Sham/Sham sequence ($\gamma_1 \rightarrow \gamma_2 \rightarrow \gamma_3$). After transfer H we perform the final electrophysiology recordings.

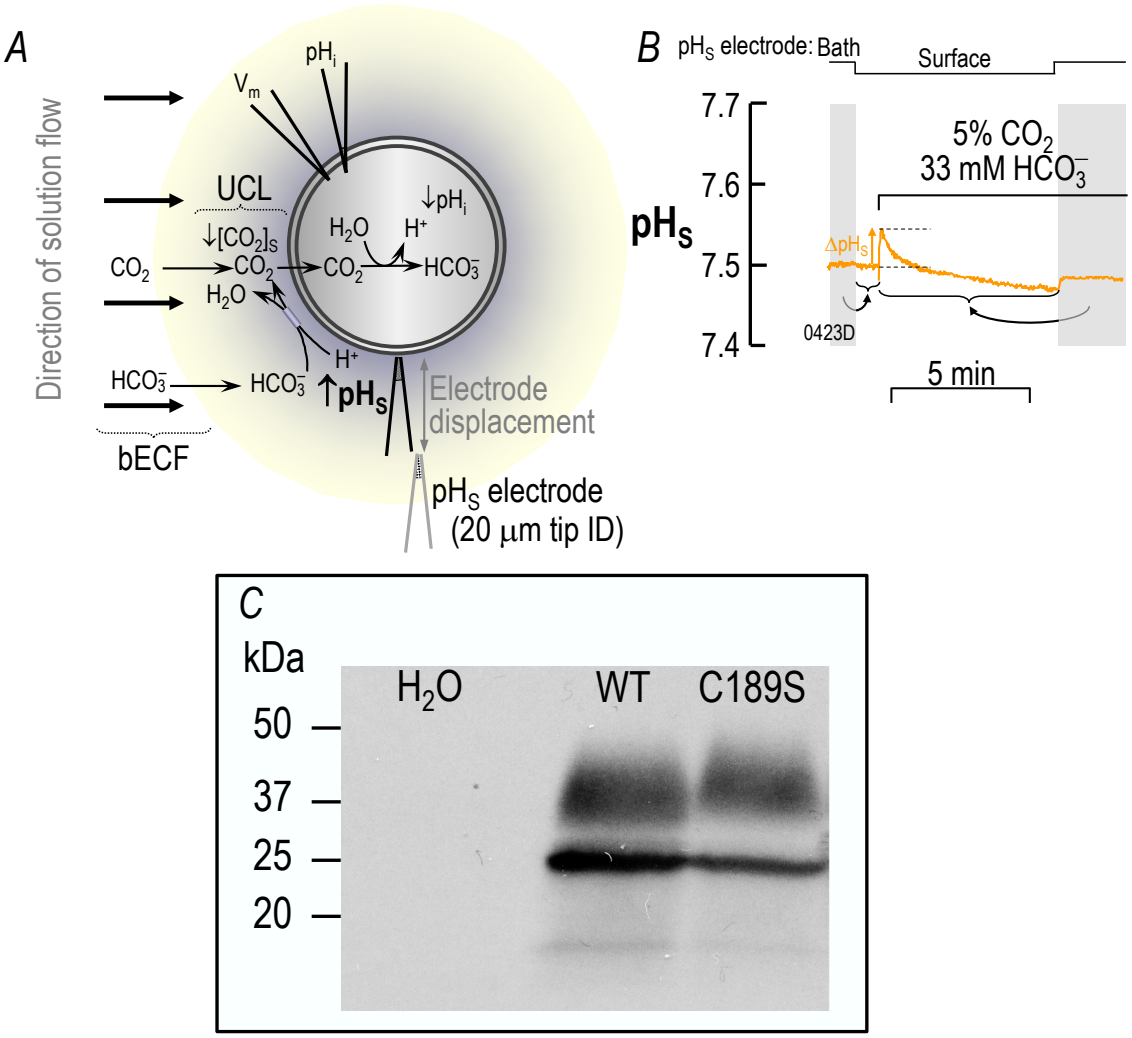

Figure 2: CO_2 influx into an oocyte.

A, schematic illustration of a CO_2-influx experiment. Thick black arrows indicate direction of convective flow within the bulk extracellular fluid (bECF). Thinner arrows indicate solute diffusion or reactions. The maize-colored halo indicates the layer of extracellular unconvected fluid (EUF). At the outer surface of the membrane, CO_2 influx creates a CO_2 deficit, in part replenished by the reaction $HCO_3^- + H^+ \rightarrow CO_2 + H_2O$ (which raises pH_S) and in part replenished by diffusion from the bECF (an isohydric process). The double-headed arrow indicates displacement of the pH_S electrode from the cell surface to the bECF for recalibration.

B, sample surface-pH (pH_S record). The upward arrow indicates the maximal change in pH_S (ΔpH_S) during the application of CO_2/HCO_3^-. During the two periods indicated by the vertical gray

bands, the tip of the pH_S electrode was displaced ~300 μm away from the cell surface for recalibration in the bulk extracellular fluid (i.e., pH = 7.50). The curved gray arrow points to horizontal braces that indicate the portions of the experiment to which each calibration pertains. The filename for this representative trace, “0423D”—that we reuse in Figure 3*A*—is annotated at the bottom left corner of the panel.

C, western blot, probed with an anti-AQP1 antibody, showing relative expression of AQP1-WT vs. AQP1-C189S in one of 3 membrane preparation of oocytes. ID, inner diameter; UCL, unconvected layer.

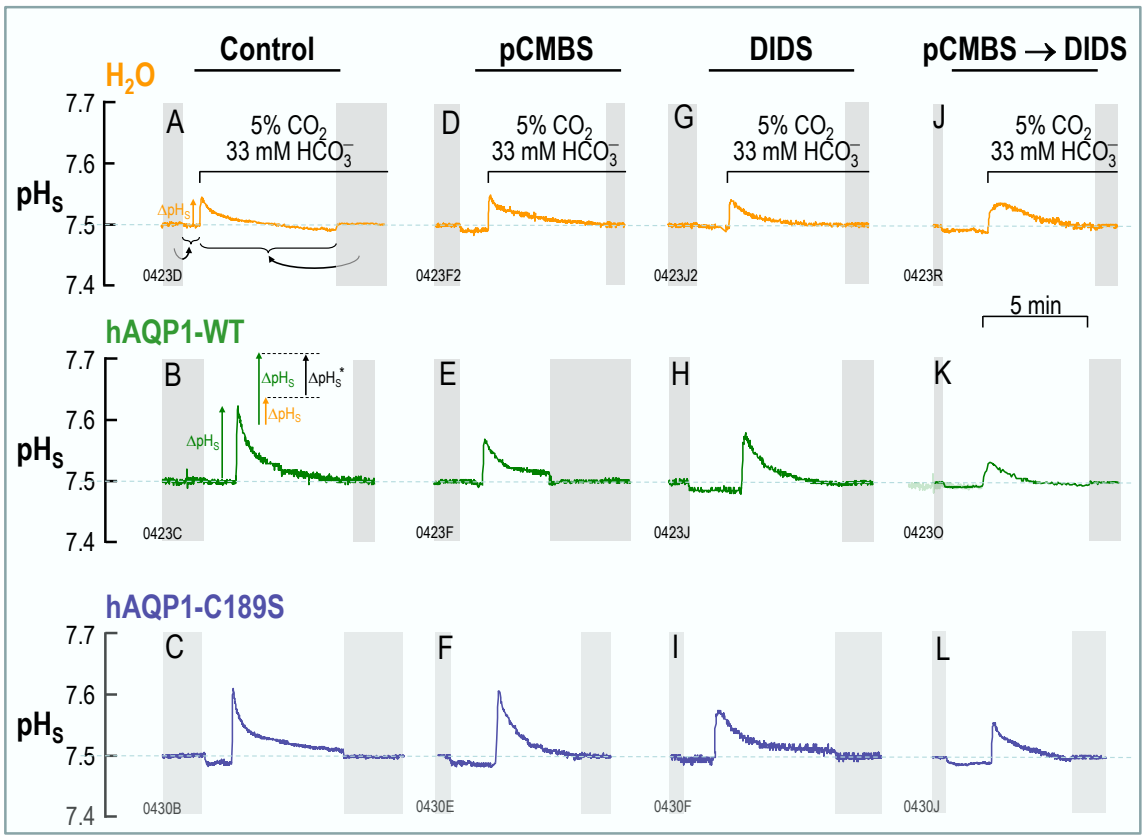

Figure 3: Surface-pH transients triggered by a CO_2/HCO_3^- exposure and subsequent CO_2 influx

The figure shows representative pH_S records from oocytes injected with H_2O (top row) or cRNA encoding hAQP1-WT (middle row) or its C189S mutant (bottom row), and later exposed first to the ND96 solution and then, at the indicated times, to a solution containing CO_2/HCO_3^-. All oocytes underwent the "Control" protocol, followed by one or two of the three indicated $F_1/F_2/F_3$ protocols in Figure 1, although some oocytes did not survive beyond the control protocol. As necessary, we pre-incubated oocytes in 1 mM pCMBS for 30 minutes, or in 100 μM DIDS for 1 hour. Neither drug was present in the bulk solution at the time of the assays. The two gray bars in each panel indicate when we withdrew the pH-electrode tip from the oocyte surface to the bulk extracellular fluid (pH 7.50) for recalibration. In panel *A*, the curved gray arrows points and horizontal braces have the same meanings as in Figure 2*B*, and the upward gold arrow indicates the control ΔpH_S. In panel *B*, the upward green arrow indicates the ΔpH_S in an oocyte expressing AQP1. The inset shows that the difference in heights of the green arrow and the gold arrow (its day-matched control) is the channel-dependent ΔpH_S (ΔpH_S*).

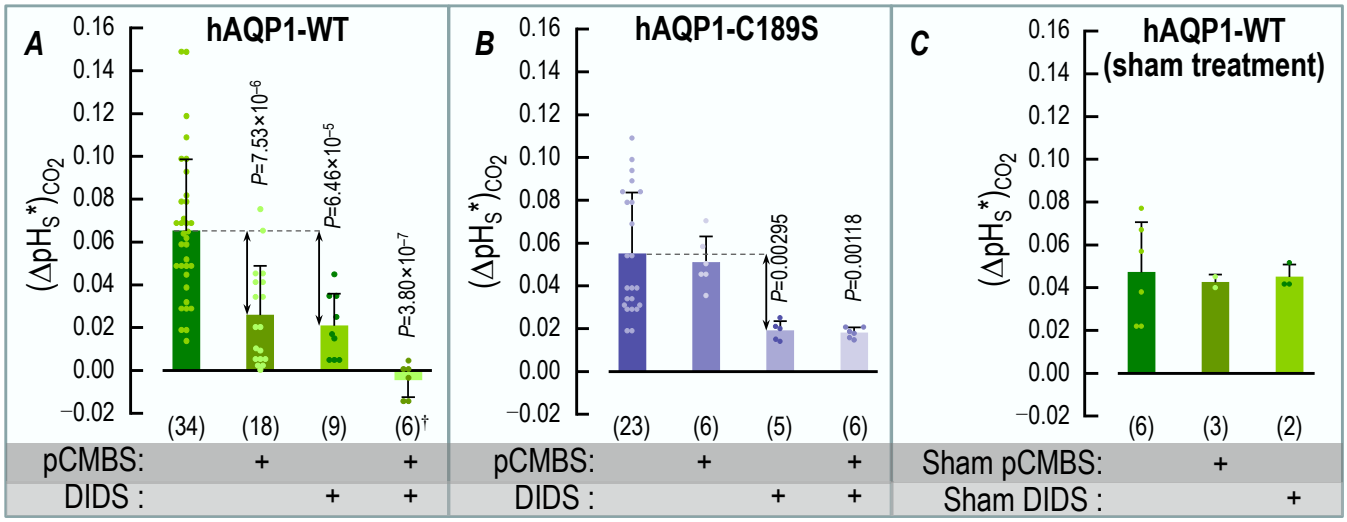

Figure 4: Summary of channel-specific data in assays for CO_2 influx

A, oocytes expressing hAQP1-WT. pCMBS and DIDS each reduces $(\Delta pH_S^*)_{CO_2}$ by somewhat more than half, and the two drugs together reduce it to virtually zero. For the rightmost bar, the dagger symbol (†) adjacent to the replicates (i.e., n = 6) indicates that the $(\Delta pH_S^*)_{CO_2}$ for the pCMBS+DIDS condition is not significantly different from zero (*P*=0.254, one-sample t-test). Of the 6 pCMBS+DIDS oocytes, 2 we treated first with pCMBS, and then DIDS; the other 4 were in the opposite order.

B, oocytes expressing the C189S mutant of hAQP1. DIDS reduces $(\Delta pH_S^*)_{CO_2}$ by about half, but pCMBS is without effect, ±DIDS. Of the 6 pCMBS+DIDS oocytes (far-right bar), 4 we treated first with pCMBS, and then DIDS; the other 2 were in the opposite order.

C, oocytes expressing AQP1 but undergoing only sham drug exposures. These sham experiments show that the long protocols did not have a substantial effect on $(\Delta pH_S^*)_{CO_2}$. The pCMBS shams (30 min) and DIDS shams (60 min) differed only in the ND96 incubation time in Figure 1/F_3.

The data come from experiments like those in Figure 3, in which we expose oocytes to 5% CO_2/33 mM HCO_3^- (for protocol, see Methods and Figure 1). From each ΔpH_S of a channel-expressing oocyte (e.g., Figure 3*B*, *E*, *H*, *K* or *C*, *F*, *I*, *L*), we subtract the mean, day-matched ΔpH_S for the corresponding H_2O-injected oocytes (e.g., Figure 3*A*, *D*, *G*, and *J*) to calculate the channel-dependent ΔpH_S for CO_2, that is, $(\Delta pH_S^*)_{CO_2}$. The $(\Delta pH_S^*)_{CO_2}$ values from individual oocytes are plotted as dots over the green-shaded bars in panels *A* and *C*, and purple-shaded

bars in panel *B*. At the base of each bar in parentheses is the numbers of oocytes (n), which come from a minimum of 5 batches of oocytes (i.e., different frogs; $N \geq 5$). Error bars represent S.D. In the horizontal gray bands at the bottom of each panel, "+" indicates a pre-incubation with pCMBS or DIDS, or a sham exposure. *P*-values denote statistically significant differences from the no-drug condition, and are results of one-way ANOVAs among all groups, followed by Holm-Bonferroni post hoc means comparisons (see Statistics in Methods). For clarity, we display only *P*-values that indicate statistical significance; we show the *P*-values for all comparisons in Statistics Table 4*A*, Statistics Table 4*B* and Statistics Table 4*C*.

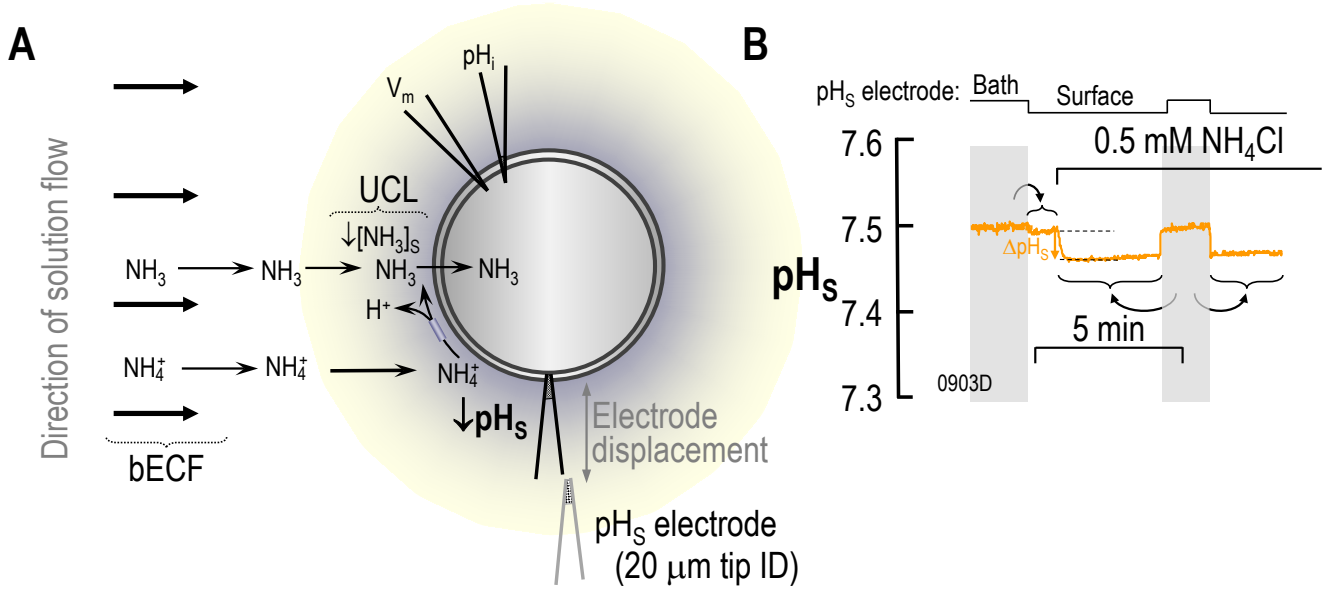

Figure 5: NH_3 influx into an oocyte.

A, schematic illustration of a NH_3-influx experiment. Analogous to Figure 2, the thick black arrows indicate the direction of convective flow within the bulk extracellular fluid (bECF). Thinner arrows indicate solute diffusion or reactions. The maize-colored halo indicates the layer of extracellular unconvected fluid (EUF). At the outer surface of the membrane, NH_3 influx creates a NH_3 deficit, in part replenished by the reaction $NH_4^+ \rightarrow NH_3 + H^+$ (which decreases pH_S) and in part replenished by diffusion from the bECF (an isohydric process). The double-headed arrow indicates movement of the pH_S electrode from the bECF to the cell surface for recalibration.

B, Example of a surface-pH (pH_S) record. The downward arrow indicates the maximal change in pH_S (ΔpH_S) during the application of NH_3/NH_4^+. During the two periods indicated by the vertical gray bands, the tip of the pH_S electrode was ~300 μm away from the cell surface for calibration in the bulk extracellular fluid (i.e., pH = 7.50). The curved gray arrows point to horizontal braces that indicate the portions of the experiment to which each calibration pertains. ID, inner diameter. The filename for this representative trace, "0903D"—that we reuse in Figure 6*A*—is annotated at the bottom left corner of the panel.

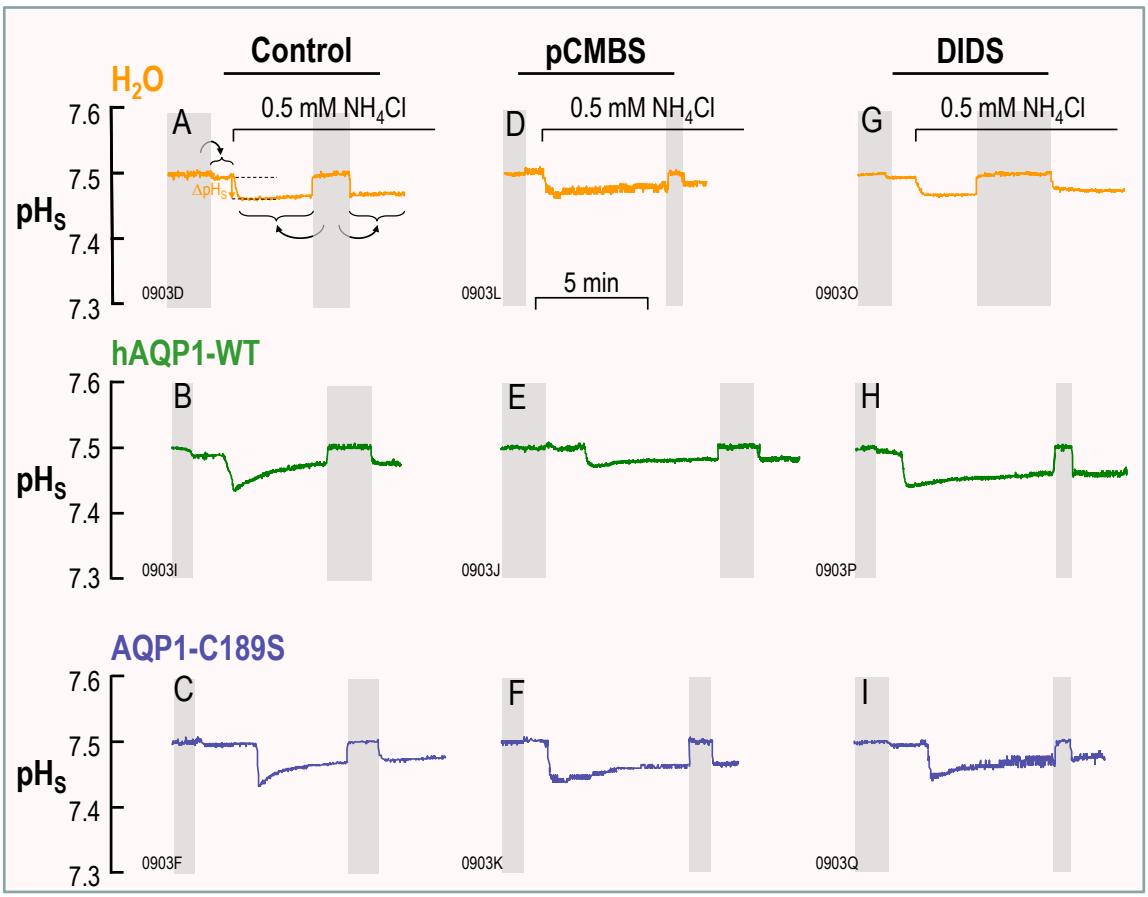

Figure 6: Surface-pH transients triggered by NH_3/NH_4^+ exposure and the subsequent NH_3 influx

The figure shows representative pH_S records from oocytes injected with H_2O (top row) or cRNA encoding hAQP1-WT (middle row) or its C189S mutant (bottom row), and later exposed first to the ND96 solution and then, at the indicated times, to a solution containing NH_3/NH_4^+. All oocytes underwent the "Control" protocol, followed by the F_1 or F_2 protocol in Figure 1, although some oocytes did not survive beyond the control protocol (see Methods). As necessary, we pre-incubated oocytes in 1 mM pCMBS for 30 min, or in 100 μM DIDS for 1 h. Neither drug was present in the bulk solution at the time of the assays. The gray bars indicate when we withdrew the pH-electrode tip from the oocyte surface to the bulk extracellular solution (pH 7.50) for recalibration. In each panel the filename the representative trace, is annotated at the bottom left corner of the panel. "0903D" in panel *A* is a reproduction of the recording in Figure 5*B*.

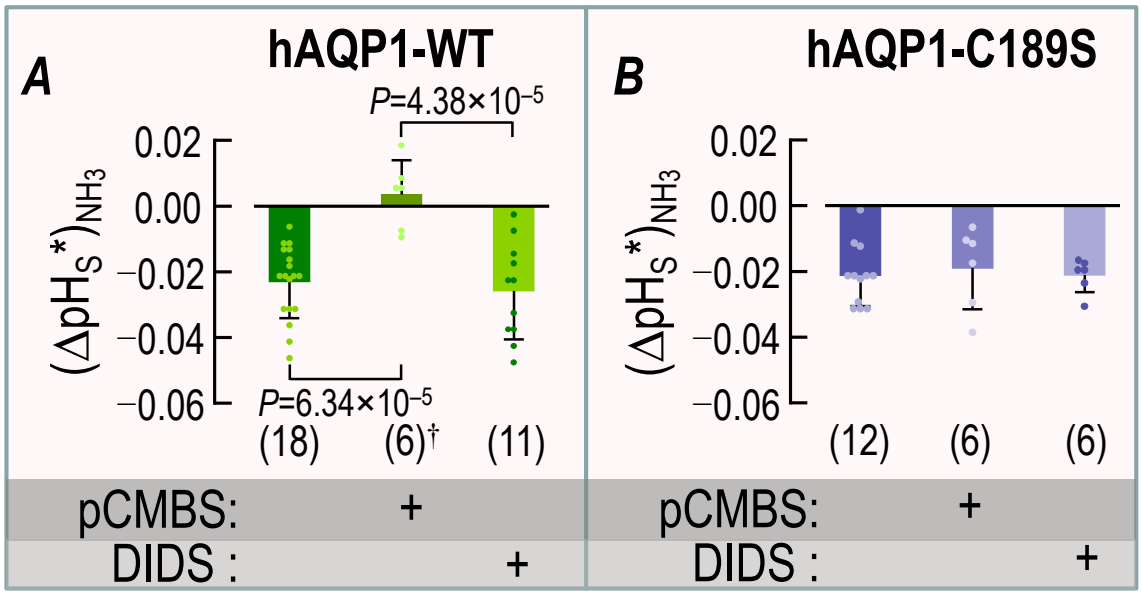

Figure 7: Summary of channel-specific data in assays for NH_3 influx

A, oocytes expressing hAQP1-WT. pCMBS reduces $(\Delta pH_S^*)_{NH_3}$ to virtually zero , whereas DIDS has no effect. For the middle bar, the dagger symbol (†) adjacent to the replicates (i.e., n = 6) indicates that the $(\Delta pH_S^*)_{NH_3}$ for the pCMBS condition is not significantly different from zero (*P*=0.450, one-sample t-test).

B, oocytes expressing the C189S mutant of hAQP1. Neither drug affects $(\Delta pH_S^*)_{NH_3}$.

The data come from experiments like those in Figure 6, in which we exposed oocytes to 0.5 mM NH_4Cl (for protocol, see Methods and Figure 1). From each ΔpH_S of a channel-expressing oocyte (Figure 6*B*, *E*, *H* or *C, F, I*), we subtracted the corresponding mean, day-matched ΔpH_S for H_2O-injected oocytes (Figure 6*A, D, G*) to calculate the channel-dependent ΔpH_S for NH_3, that is, $(\Delta pH_S^*)_{NH_3}$. The $(\Delta pH_S^*)_{NH_3}$ values from individual oocytes are plotted over the green-shaded bars in panel *A*, and purple-shaded bars in panel *B*. At the base of each bar in parentheses is the number of oocytes (n), which come from a minimum of 5 batches of oocytes (i.e., different frogs; *N*). Error bars represent S.D. In the horizontal gray bands at the bottom of each panel, "+" indicates a pre-incubation with pCMBS or DIDS. *P*-values denote statistically significant differences from the no-drug condition, and are the results of one-way ANOVAs among all groups, followed by Holm-Bonferroni post-hoc means comparisons (see Statistics in Methods). For clarity, we display only *P*-values that indicate statistical significance; we show *P*-values for all comparisons in Statistics Table 7*A* and Statistics Table 7*B*.

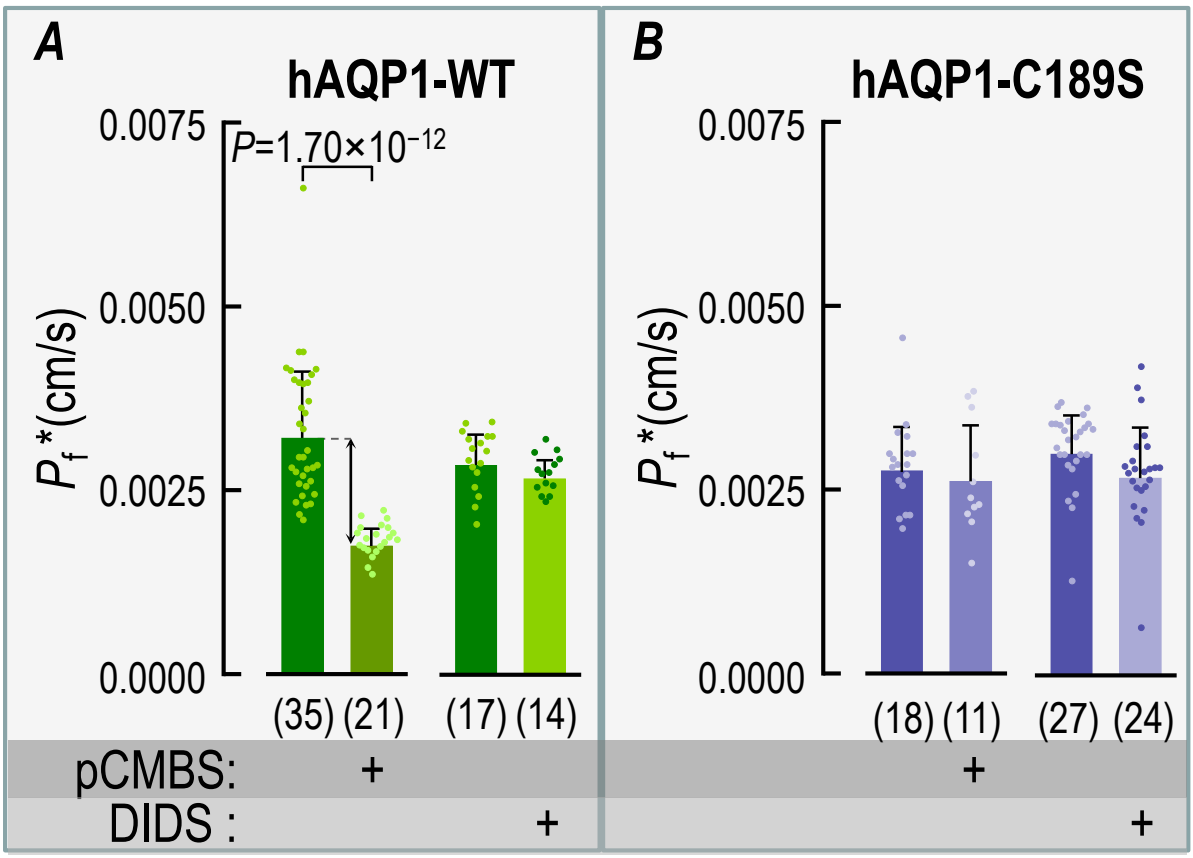

Figure 8: Summary of channel-specific data in assays for osmotic water permeability

A, oocytes expressing hAQP1-WT. pCMBS but not DIDS reduces P_f.

B, oocytes expressing the C189S mutant of hAQP1. Neither drug reduces P_f.

From each P_f from a channel-expressing oocyte, we subtracted the corresponding mean, day-matched P_f for H_2O-injected oocytes to calculate the channel-dependent P_f, that is, P_f*. The P_f* values from individual oocytes are plotted over the green-shaded bars in panel *A*, and purple-shaded bars in panel *B*. At the base of each bar in parentheses is the number of oocytes (n), which come from a minimum of 5 batches of oocytes (i.e., different frogs; *N*). Error bars represent S.D. In the horizontal gray bands at the bottom of each panel, "+" indicates a pre-incubation with pCMBS or DIDS. *P*-values denote statistically significant differences from the no-drug condition, and are the results of a one-way ANOVAs among all groups, followed by Holm-Bonferroni post-hoc means comparisons (see Statistics in Methods). For clarity, we display only *P*-values that indicate statistical significance; we show *P*-values for all comparisons in Statistics Table 8.

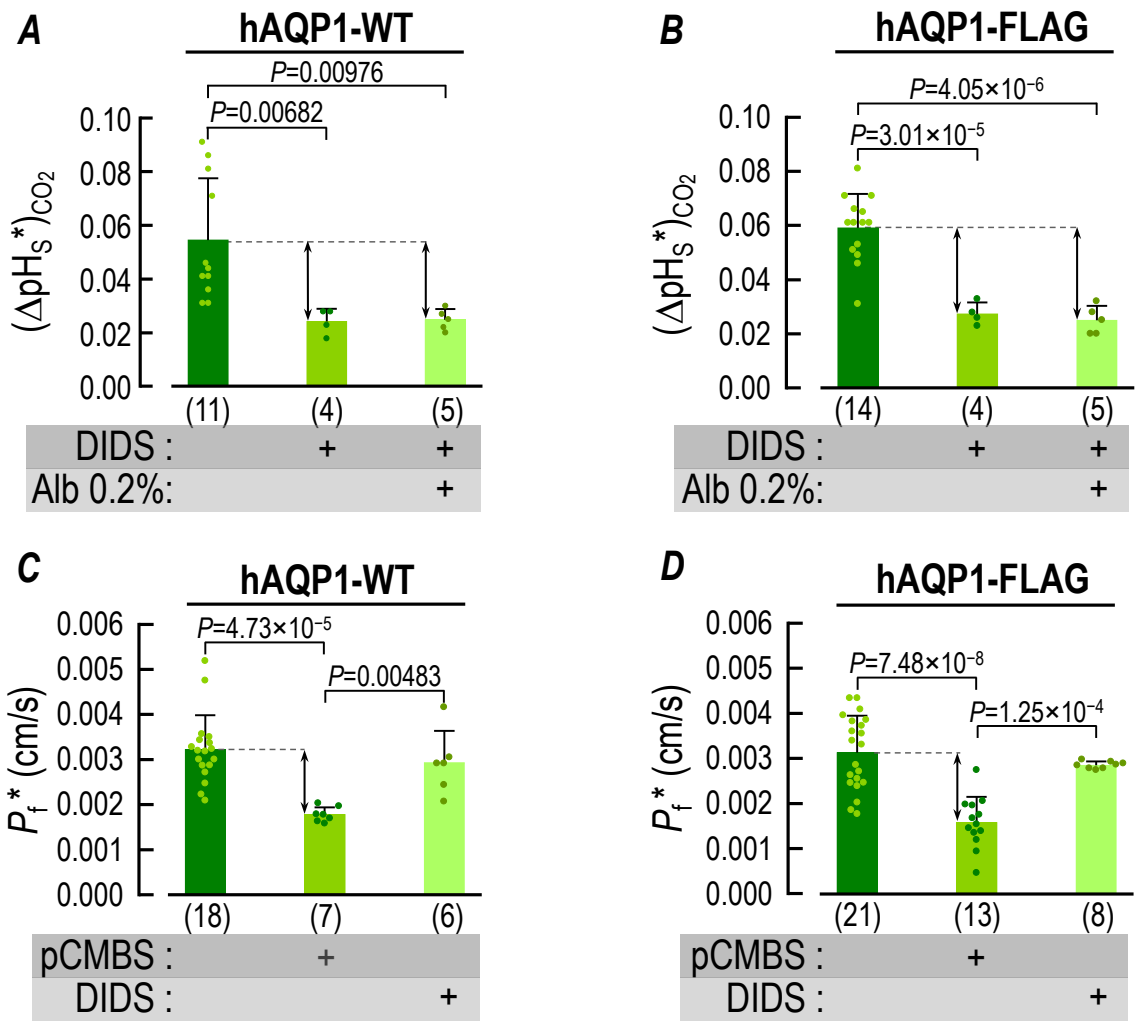

Figure 9: Summary of channel-specific data for CO_2 and H_2O influx for WT vs. FLAG-tagged hAQP1

A, oocytes expressing hAQP1-WT: effect of albumin washes on the DIDS sensitivity of $(\Delta pH_S^*)_{CO_2}$. DIDS reduces $(\Delta pH_S^*)_{CO_2}$ by about half, regardless of the albumin wash.

B, oocytes expressing N-terminally FLAG-tagged hAQP1: effect of albumin washes on the DIDS sensitivity of $(\Delta pH_S^*)_{CO_2}$. Also in the FLAG-tagged construct, DIDS reduces $(\Delta pH_S^*)_{CO_2}$ by about half, regardless of the albumin wash.

C, oocytes expressing hAQP1-WT: effect of albumin washes on the DIDS sensitivity of P_f^*. These experiments are a matched control for the study in panel *D*. As in the comparable experiments summarized in Figure 8*A*, pCMBS but not DIDS reduces P_f.

D, oocytes expressing FLAG-tagged hAQP1: effect of albumin washes on the DIDS sensitivity of P_f*. As in panel *C* (no FLAG tag), pCMBS but not DIDS reduces P_f in oocytes expressing FLAG-tagged hAQP1.

For panels *A* and *B*, the control pH_S data (leftmost dark-green bars) come from experiments like those in Figure 3, whereas for panels *C* and *D*, the control P_f data come from experiments like those in Figure 8. The $(\Delta pH_S^*)_{CO_2}$ or P_f* values from individual oocytes are plotted as dots over the green-shaded bars in panels *A* through *D*. At the base of each bar in parentheses is the numbers of oocytes (n), which come from a minimum of 5 batches of oocytes (i.e., different frogs; $N \geq 5$). Error bars represent S.D. In the horizontal gray bands at the bottom of each panel, "+" indicates a pre-incubation with pCMBS or DIDS, or the presence of 0.2% bovine serum albumin (Alb 0.2%) *P*-values denote statistically significant differences from the no-drug condition, and are results of one-way ANOVAs among all groups, followed by Holm-Bonferroni means comparisons (see Statistics in Methods). For clarity, we display only the *P*-values that indicate statistical significance; we show *P*-values for all comparisons in Statistics Table 9.

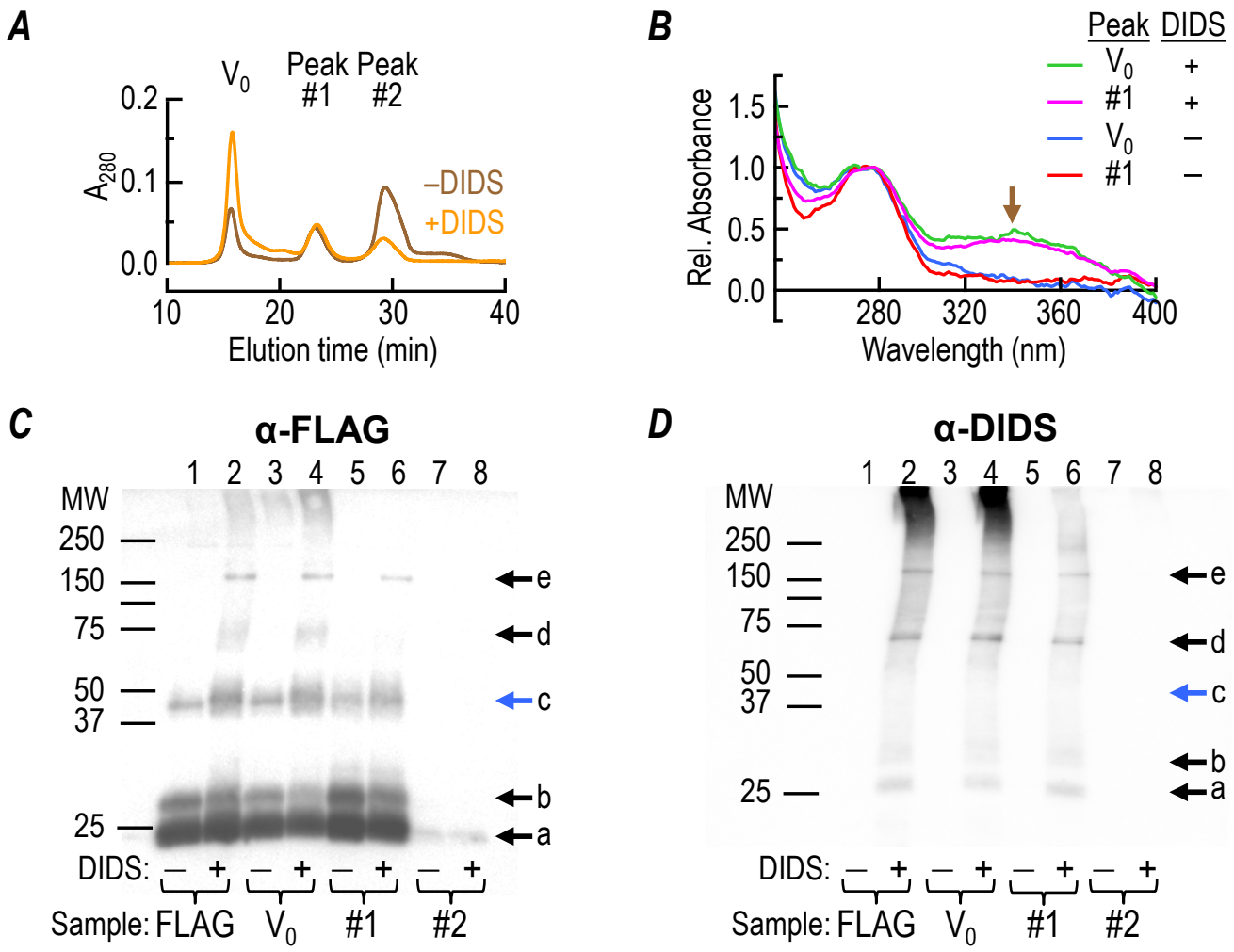

Figure 10: Reaction of DIDS with N-terminally FLAG-tagged hAQP1 overexpressed in *Pichia pastoris*

A, Size-exclusion chromatography of solubilized proteins. We treated spheroplasts with DIDS (or no DIDS in parallel, sham experiments), solubilized with DMM, purified N-terminally FLAG-tagged hAQP1-WT using an anti-FLAG column, and then separated by FPLC on a Superdex-200 column, recording A_{280} vs. time. The orange record represents a DIDS-treated sample and the brown record, a control sample (–DIDS) from the same preparation. The first peaks are the void volume (V_0), which consists of high molecular-weight (MW) proteins. Peak #1 consists of lower-MW proteins, and Peak #2, even smaller ones. We translated both records to so that A_{280} averaged zero between 10 and 13 min, and then we scaled the orange +DIDS record to that it has the same total area under the curve as Peak #1 in the –DIDS record.

B, Absorbance spectra of material (±DIDS) from peaks V_0 and #1, from a preparation similar to that shown in panel *A*. We normalized all spectra to unity at 280 nm. The increased absorbance from ~320 to ~370 nm in the DIDS-treated samples presumably represents DIDS, which has an absorbance peak at ~340 nm (Kodippili et al., 2009).

C, Western blot of material from the same experiment as in panel *B*, probed with anti-FLAG: Lane 1. Material obtained from spheroplasts not treated with DIDS, and purified on anti-FLAG column, as described for panel *A*, but not subjected to size-exclusion chromatography. ||| Lane 2. Same as Lane 1, but from DIDS-treated spheroplasts ||| Lane 3. Peak V_0 from spheroplasts –DIDS ||| Lane 4. Same as Lane 3, but from spheroplasts +DIDS ||| Lane 5. Peak #1 from spheroplasts –DIDS ||| Lane 6. Same as Lane 5, but from spheroplasts +DIDS ||| Lane 7. Peak #2 from spheroplasts –DIDS ||| Lane 8. Same as Lane 7, but from spheroplasts +DIDS. The presumed assignments are: “a” band < 25 kDa, unglycosylated AQP1 monomer cleaved in the C-terminus; band “b”, 28 kDa, full-length unglycosylated monomer; band “c”, glycosylated monomer (blue arrow); band “d”, glycosylated dimer; band “e”, glycosylated tetramer.

D, Western blot of material from the same experiment as in panels *B* and *C*, probed with anti-DIDS. The lane assignments are the same as in panel *C*. The results in panels *A* through *D* are representative of two independent experiments.

Tables

Table 1 Solutions*

Solution / Component or parameter	1	2	3	4	5	6	7	8	9
	ND96	Ca^{2+}-free ND96	5% CO_2/ 33 mM HCO_3^- [for $(\Delta pH_S)_{CO_2}$]	5 mM NH_3/NH_4^+ in ND96	0.5 mM NH_3/NH_4^+ in ND96 [for $(\Delta pH_S)_{NH3}$]	Hypotonic ND96 [for P_f]	ND96 + pCMBS	ND96 + DIDS	BSA [to scavenge DIDS]
NaCl (mM)	96	98.7	63	91	91	33	96	96	96
KCl (mM)	2.0	2.0	2.0	2.0	2.0	2.0	2.0	2.0	2.0
$CaCl_2$ (mM)	1.8	0	1.8	1.8	1.8	1.8	1.8	1.8	1.8
$MgCl_2$ (mM)	1.0	1.0	1.0	1.0	1.0	1.0	1.0	1.0	1.0
HEPES (mM)	5	5	5	5	5	5	5	5	5
$NaHCO_3$ (mM)	0	0	33	0	0	0	0	0	0
NH_4Cl (mM)	0	0	0	5	0.5	0	0	0	0
CO_2 (%)	0	0	5	0	0	0	0	0	0
pH (adjusted with NaOH)	~7.50	~7.50	~7.50	~7.50	~7.50	~7.50	~7.50	~7.50	~7.50
Temperature (°C)	RT	RT	RT	RT	RT	RT	RT	RT	RT
Osmolality (mOsm)	~195	~195	~195	~195	~195	~80	~195	~195	~195
pCMBS (mM)	0	0	0	0	0	0	1	0	0
DIDS (μM)	0	0	0	0	0	0	0	100	0
BSA %	0	0	0	0	0	0	0	0	0.2%

*This table shows the compositions of all the solutions used in the physiology experiments the present paper.

Abbreviations: BSA, Bovine serum albumin; DIDS, 4,4'-diisothiocyanatostilbene-2,2'-disulfonate; pCMBS, p-chloromercuribenzene sulfonate, P_f, osmotic water permeability

References

Al-Samir S, Kyriazi D, Yool AJ, Moser I, Kyriazi K, Gros G, Tsiavaliaris G & Endeward V (2025). Aquaporin-1 acts as an O_2 channel. The permeability of human and mouse red cell membranes for oxygen. *Am J Physiol Cell Physiol*; DOI: 10.1152/ajpcell.00858.2024.

Ammann D, Lanter F, Steiner RA, Schulthess P, Shijo Y & Simon W (1981). Neutral carrier based hydrogen ion selective microelectrode for extra- and intracellular studies. *Anal Chem* **53,** 2267–2269.

Assentoft M, Kaptan S, Schneider H-P, Deitmer JW, de Groot BL & MacAulay N (2016). Aquaporin 4 as a NH_3 channel. *J Biol Chem* **291,** 19184–19195.

Boron WF (2010). Sharpey-Schafer lecture: Gas channels. *Exp Physiol* **95,** 1107–1130.

Boron WF, Endeward V, Gros G, Musa-Aziz R & Pohl P (2011). Intrinsic CO_2 permeability of cell membranes and potential biological relevance of CO_2 channels. *Chemphyschem Eur J Chem Phys Phys Chem* **12,** 1017–1019.

Cabantchik ZI & Rothstein A (1972). The nature of the membrane sites controlling anion permeability of human red blood cells as determined by studies with disulfonic stilbene derivatives. *J Membr Biol* **10,** 311–330.

Calvetti D, Prezioso J, Occhipinti R, Boron WF & Somersalo E (2020). Computational model of electrode-induced microenvironmental effects on pH measurements near a cell membrane. *SIAM Multiscale Model Simul* **18,** 1053–1075.

Chandy G, Zampighi GA, Kreman M & Hall JE (1997). Comparison of the water transporting properties of MIP and AQP1. *J Membr Biol* **159,** 29–39.

Cooper GJ & Boron WF (1998). Effect of pCMBS on CO_2 permeability of *Xenopus* oocytes expressing aquaporin 1 or its C189S mutant. *Am J Physiol* **275,** C1481-1486.

Endeward V, Cartron J-P, Ripoche P & Gros G (2008). RhAG protein of the Rhesus complex is a CO_2 channel in the human red cell membrane. *FASEB J* **22,** 64–73.

Endeward V, Musa-Aziz R, Cooper GJ, Chen L-M, Pelletier MF, Virkki LV, Supuran CT, King LS, Boron WF & Gros G (2006). Evidence that aquaporin 1 is a major pathway for CO_2 transport across the human erythrocyte membrane. *FASEB J* **20,** 1974–1981.

Forster RE, Gros G, Lin L, Ono Y & Wunder M (1998). The effect of 4,4'-diisothiocyanato-stilbene-2,2'-disulfonate on CO_2 permeability of the red blood cell membrane. *Proc Natl Acad Sci U S A* **95,** 15815–15820.

Garcia AM & Lodish HF (1989). Lysine 539 of human band 3 is not essential for ion transport or inhibition by stilbene disulfonates. *J Biol Chem* **264,** 19607–19613.

Geyer RR, Musa-Aziz R, Qin X & Boron WF (2013). Relative CO_2/NH_3 selectivities of mammalian aquaporins 0-9. *Am J Physiol Cell Physiol* **304,** C985-994.

Gomes D, Agasse A, Thiébaud P, Delrot S, Gerós H & Chaumont F (2009). Aquaporins are multifunctional water and solute transporters highly divergent in living organisms. *Biochim Biophys Acta* **1788,** 1213–1228.

Gustin MC, Albertyn J, Alexander M & Davenport K (1998). MAP kinase pathways in the yeast Saccharomyces cerevisiae. *Microbiol Mol Biol Rev MMBR* **62,** 1264–1300.

Herrera M, Hong NJ & Garvin JL (2006). Aquaporin-1 transports NO across cell membranes. *Hypertension* **48,** 157–164.

Holm S (1979). A simple sequentially rejective multiple test procedure. *Scand J Stat* **6,** 65–70.

Kabutomori J, Beloto-Silva O, Geyer RR & Musa-Aziz R (2018). Lithobates catesbeianus (American Bullfrog) oocytes: a novel heterologous expression system for aquaporins. *Biol Open*; DOI: 10.1242/bio.031880.

Kodippili GC, Spector J, Sullivan C, Kuypers FA, Labotka R, Gallagher PG, Ritchie K & Low PS (2009). Imaging of the diffusion of single band 3 molecules on normal and mutant erythrocytes. *Blood* **113,** 6237–6245.

Leduc-Nadeau A, Lahjouji K, Bissonnette P, Lapointe J-Y & Bichet DG (2007). Elaboration of a novel technique for purification of plasma membranes from Xenopus laevis oocytes. *Am J Physiol Cell Physiol* **292,** C1132-1136.

Lepke S, Fasold H, Pring M & Passow H (1976). A study of the relationship between inhibition of anion exchange and binding to the red blood cell membrane of 4,4'-diisothiocyano stilbene-2,2'-disulfonic acid (DIDS) and its dihydro derivative (H_2DIDS). *J Membr Biol* **29,** 147–177.

Macey RI (1984). Transport of water and urea in red blood cells. *Am J Physiol* **246,** C195-203.

Michenkova M, Taki S, Blosser MC, Hwang HJ, Kowatz T, Moss FJ, Occhipinti R, Qin X, Sen S, Shinn E, Wang D-K, Zeise B, Zhao P, Malmstadt N, Vahedi-Faridi A, Tajkhorshid E & Boron WF (2021). Carbon dioxide transport across membranes. *Interface Focus* **11,** 2.

Moss FJ, Zhao P, Salameh AI, Taki S, Wass AB, Jacobberger JW, Huffman DE, Meyerson HJ, Occhipinti R & Boron WF (2025). Role of channels in the O_2 permeability of murine red blood cells II. Morphological and proteomic studies. *bioRxiv*; DOI: 10.1101/2025.03.05.639962.

Musa-Aziz R, Boron WF & Parker MD (2010). Using fluorometry and ion-sensitive microelectrodes to study the functional expression of heterologously-expressed ion channels and transporters in *Xenopus* oocytes. *Methods San Diego Calif* **51,** 134–145.

Musa-Aziz R, Chen L-M, Pelletier MF & Boron WF (2009*a*). Relative CO_2/NH_3 selectivities of AQP1, AQP4, AQP5, AmtB, and RhAG. *Proc Natl Acad Sci U S A* **106,** 5406–5411.

Musa-Aziz R, Jiang L, Chen L-M, Behar KL & Boron WF (2009*b*). Concentration-dependent effects on intracellular and surface pH of exposing *Xenopus* oocytes to solutions containing NH_3/NH_4^+. *J Membr Biol* **228,** 15–31.

Musa-Aziz R, Occhipinti R & Boron WF (2014*a*). Evidence from simultaneous intracellular- and surface-pH transients that carbonic anhydrase II enhances CO_2 fluxes across *Xenopus* oocytes plasma membranes. *Am J Physiol Cell Physiol* **307,** C791-813.

Musa-Aziz R, Occhipinti R & Boron WF (2014*b*). Evidence from simultaneous intracellular- and surface-pH transients that carbonic anhydrase IV enhances CO_2 fluxes across *Xenopus* oocyte plasma membranes. *Am J Physiol Cell Physiol* **307,** C814-840.

Nakhoul NL, Davis BA, Romero MF & Boron WF (1998). Effect of expressing the water channel aquaporin-1 on the CO_2 permeability of *Xenopus* oocytes. *Am J Physiol* **274,** C543-548.

Nakhoul NL, Hering-Smith KS, Abdulnour-Nakhoul SM & Hamm LL (2001). Transport of NH_3/NH_4^+ in oocytes expressing aquaporin-1. *Am J Physiol Renal Physiol* **281,** F255-263.

Occhipinti R, Musa-Aziz R & Boron WF (2014). Evidence from mathematical modeling that carbonic anhydrase II and IV enhance CO_2 fluxes across *Xenopus* oocytes plasma membranes. *Am J Physiol Cell Physiol* **307,** C841-858.

Occhipinti R, Zhao P, Moss FJ & Boron WF (2025). Role of channels in the O_2 permeability of murine red blood cells. III. Mathematical modeling and simulations. *bioRxiv*; DOI: 10.1101/2025.03.05.639964.

Prasad GV, Coury LA, Finn F & Zeidel ML (1998). Reconstituted aquaporin 1 water channels transport CO_2 across membranes. *J Biol Chem* **273,** 33123–33126.

Preston GM & Agre P (1991). Isolation of the cDNA for erythrocyte integral membrane protein of 28 kilodaltons: member of an ancient channel family. *Proc Natl Acad Sci U S A* **88,** 11110–11114.

Preston GM, Carroll TP, Guggino WB & Agre P (1992). Appearance of water channels in *Xenopus* oocytes expressing red cell CHIP28 protein. *Science* **256,** 385–387.

Preston GM, Jung JS, Guggino WB & Agre P (1993). The mercury-sensitive residue at cysteine 189 in the CHIP28 water channel. *J Biol Chem* **268,** 17–20.

Roos A & Boron WF (1981). Intracellular pH. *Physiol Rev* **61,** 296–434.

Rumble JR ed. (2022). *CRC handbook of chemistry and physics. a ready-reference book of chemical and physical data*, 103rd edition, 2022-2023. CRC Press.

Somersalo E, Occhipinti R, Boron WF & Calvetti D (2012). A reaction-diffusion model of CO_2 influx into an oocyte. *J Theor Biol* **309,** 185–203.

Sui H, Han BG, Lee JK, Walian P & Jap BK (2001). Structural basis of water-specific transport through the AQP1 water channel. *Nature* **414,** 872–878.

Tajkhorshid E, Nollert P, Jensen MØ, Miercke LJW, O'Connell J, Stroud RM & Schulten K (2002). Control of the selectivity of the aquaporin water channel family by global orientational tuning. *Science* **296,** 525–530.

Trudeau MC, Warmke JW, Ganetzky B & Robertson GA (1995). HERG, a human inward rectifier on the voltage-gated potassium channel family. *Science* **269,** 92–95.

Uehlein N, Lovisolo C, Siefritz F & Kaldenhoff R (2003). The tobacco aquaporin NtAQP1 is a membrane CO_2 pore with physiological functions. *Nature* **425,** 734–737.

Verkman AS (2008). Mammalian aquaporins: diverse physiological roles and potential clinical significance. *Expert Rev Mol Med* **10,** e13.

Verkman AS, Ruiz-Ederra J & Levin MH (2008). Functions of aquaporins in the eye. *Prog Retin Eye Res* **27,** 420–433.

Virkki LV, Cooper GJ & Boron WF (2001). Cloning and functional expression of an MIP (AQP0) homolog from killifish (Fundulus heteroclitus) lens. *Am J Physiol Regul Integr Comp Physiol* **281,** R1994-2003.

Waisbren SJ, Geibel JP, Modlin IM & Boron WF (1994). Unusual permeability properties of gastric gland cells. *Nature* **368,** 332–335.

Walz T, Hirai T, Murata K, Heymann JB, Mitsuoka K, Fujiyoshi Y, Smith BL, Agre P & Engel A (1997). The three-dimensional structure of aquaporin-1. *Nature* **387,** 624–627.

Wang C, Hu H, Qin X, Zeise B, Xu D, Rappel W-J, Boron WF & Schroeder JI (2016). Reconstitution of CO_2 regulation of SLAC1 anion channel and function of CO_2-permeable PIP2;1 aquaporin as carbonic anhydrase 4 interactor. *Plant Cell* **28,** 568–582.

Wang D-K & Boron WF (2025). Manipulating the CO_2/H_2O selectivity of human aquaporin 5 through mutagenesis. *Submitt*.

Wang Y, Cohen J, Boron WF, Schulten K & Tajkhorshid E (2007). Exploring gas permeability of cellular membranes and membrane channels with molecular dynamics. *J Struct Biol* **157,** 534–544.

Zeidel ML, Nielsen S, Smith BL, Ambudkar SV, Maunsbach AB & Agre P (1994). Ultrastructure, pharmacologic inhibition, and transport selectivity of aquaporin channel-forming integral protein in proteoliposomes. *Biochemistry* **33,** 1606–1615.

Zhang RB, Logee KA & Verkman AS (1990). Expression of mRNA coding for kidney and red cell water channels in *Xenopus* oocytes. *J Biol Chem* **265,** 15375–15378.

Zhao P, Moss FJ, Occhipinti R, Geyer RR, Huffman DE, Meyerson HJ & Boron W F (2025). Role of channels in the O_2 permeability of murine red blood cells. I. Stopped-flow and hematological studies. *bioRxiv*; DOI: 10.1101/2025.03.05.639948.

Zwiazek JJ, Xu H, Tan X, Navarro-Ródenas A & Morte A (2017). Significance of oxygen transport through aquaporins. *Sci Rep* **7,** 40411.

Statistics tables

Statistics Table 4: Tables of *P*-values for one-way ANOVA with Holm-Bonferroni post-hoc means comparison for comparisons of differences of channel corrected $(\Delta pH_S^*)_{CO_2}$ on exposure of the oocytes to 5% CO_2/33 mM HCO_3^-. Each table is split in two halves, with FWER α set at 0.05, the upper-right half shows the adjusted α-value for each comparison and the lower-left half the *P*-value. Significant *P*-values are highlighted bold.

Statistics Table 4*A*: Statistics summary of channel-specific data in assays for CO_2-influx into AQP1 expressing oocytes treated with pCMBS, DIDS or pCMBS and DIDS in Figure 4*A*

AQP1		Ctrl	+pCMBS	+DIDS	+pCMBS & +DIDS
	P \ α		α	α	α
Ctrl			0.0100	0.0125	0.00833
+pCMBS	***P***	**7.53×10^{-6}**		0.0500	0.0167
+DIDS	***P***	**6.46×10^{-5}**	0.657		0.0250
+pCMBS & +DIDS	***P***	**3.80×10^{-7}**	0.0242	0.0902	

Statistics Table 4*B*: Statistics summary of channel-specific data in assays for CO_2-influx into AQP1-C198S expressing oocytes treated with pCMBS, DIDS or pCMBS and DIDS in Figure 4*B*

AQP1-C188S		Ctrl	+pCMBS	+DIDS	+pCMBS & +DIDS
	P \ α		α	α	α
Ctrl			0.0250	0.0100	0.00833
+pCMBS	***P***	0.696		0.0167	0.0125
+DIDS	***P***	**0.00295**	0.0273		0.0500
+pCMBS & +DIDS	***P***	**0.00118**	0.0177	0.946	

Statistics Table 4*C*: Statistics summary of channel-specific data in assays for CO_2-influx into AQP1 expressing oocytes incubated with sham pCMBS, or sham DIDS treatments in Figure 4*C*

AQP1		Ctrl	Sham +pCMBS	Sham +DIDS
	P \ α		α	α
Ctrl			0.0167	0.0250
Sham +pCMBS	***P***	0.768		0.0500
Sham +DIDS	***P***	0.874	0.887	

Statistics Table 7 Tables of *P*-values for one-way ANOVA with Holm-Bonferroni post-hoc means comparison for comparisons of differences of channel corrected $(\Delta pH_S^*)_{NH_3}$ on exposure of the oocytes to 0.5 mM NH_4Cl. Each table is split in two halves by the black-shaded cells, with FWER α set at 0.05, the upper-right half shows the adjusted α-value for each comparison and the lower-left half the *P*-value. Significant *P*-values are highlighted bold.

Statistics Table 7*A* Statistics summary of channel-specific data in assays for NH_3 influx into AQP1 expressing oocytes treated with pCMBS, or DIDS in Figure 7*A*

AQP1	P \ α	Ctrl	+pCMBS	+DIDS
			α	α
Ctrl			0.0250	0.0500
+pCMBS	***P***	6.34×10–5		0.0167
+DIDS	***P***	0.551	4.38×10–5	

Statistics Table 7*B* Statistics summary of channel-specific data in assays for NH_3 influx into AQP1-C189S expressing oocytes treated with pCMBS, or DIDS in Figure 7*B*

AQP1-C189S	*P* \ α	Ctrl	+pCMBS	+DIDS
			α	α
Ctrl			0.0167	0.0500
+pCMBS	***P***	0.636		0.0250
+DIDS	***P***	0.984	0.694	

Statistics Table 8 for Figure 8 Tables of *P*-values for one-way ANOVA with Holm-Bonferroni post-hoc means comparison for comparisons of differences of channel corrected P_f^* after incubation in no drug control (Ctrl), +pCMBS or +DIDS solutions. Ctrl oocytes are separated into two groups. Those from the same oocyte preparations (frogs) pre-incubated with pCMBS and those from the same oocyte preparations pre-incubated with DIDS. Each table is split in two halves by the black-shaded cells, with FWER α set at 0.05, the upper-right half shows the adjusted α-value for each comparison and the lower-left half the *P*-value. Significant *P*-values are highlighted bold. Cells shaded gray are comparisons between conditions performed on oocytes from different frogs, therefore the comparisons are not pertinent even if the *P*-value is statistically significant.

Statistics Table 8*A* Statistics summary channel-specific P_f data in assays for osmotic water permeability for AQP1 oocytes in Figure 8*A*

AQP1		Ctrl for +pCMBS	+pCMBS	Ctrl for +DIDS	+DIDS
	P \ α		α	α	α
Ctrl for +pCMBS			0.00833	0.0250	0.0167
+pCMBS	*P*	**1.70×10^{-12}**		0.0100	0.0125
Ctrl for +DIDS	*P*	0.0632	**9.02×10^{-7}**		0.0500
+DIDS	*P*	**0.00761**	**8.72×10^{-5}**	0.395	

Statistics Table 8*B* summary channel-specific P_f data in assays for osmotic water permeability for AQP1-C189S oocytes in Figure 8*B*

AQP1-C189S		Ctrl for +pCMBS	+pCMBS	Ctrl for +DIDS	+DIDS
	P \ α		α	α	α
Ctrl for +pCMBS			0.0167	0.0125	0.0500
+pCMBS	*P*	0.514		0.0100	0.0250
Ctrl for +DIDS	*P*	0.171	0.0644		0.00833
+DIDS	*P*	0.722	0.702	0.0619	

Statistics Table 9 for Figure 9 Tables of *P*-values for one-way ANOVA with Holm-Bonferroni post-hoc means comparison for comparisons of differences in channel corrected ***A,*** $(\Delta pH_S^*)_{CO_2}$ in WT AQP1 oocytes, ***B,*** $(\Delta pH_S^*)_{CO_2}$ in AQP1-FLAG tagged oocytes, ***C,*** P_f^* in WT AQP1 oocytes, and ***D,*** P_f^* in AQP1-FLAG tagged oocytes. Each table is split in two halves by the black-shaded cells, with FWER α set at 0.05, the upper-right half shows the adjusted α-value for each comparison and the lower-left half the *P*-value. Significant *P*-values are highlighted bold.

Statistics Table 9*A* Statistics summary of channel-specific CO_2 influx data for into WT AQP1 oocytes

AQP1		Ctrl	+DIDS	+DIDS +Alb 0.2%
	P \ α		α	α
Ctrl			0.0250	0.0167
+DIDS	***P***	**0.00976**		0.0500
+DIDS +Alb 0.2%	***P***	**0.00682**	0.955	

Statistics Table 9*B* Statistics summary of channel-specific CO_2 influx data for into AQP1-FLAG oocytes

AQP1-FLAG		Ctrl	+DIDS	+DIDS +Alb 0.2%
	P \ α		α	α
Ctrl			0.0250	0.0167
+DIDS	***P***	**3.01×10^{-5}**		0.0500
+DIDS +Alb 0.2%	***P***	**4.05×10^{-6}**	0.740	

Statistics Table 9*C* Statistics summary of channel-specific P_f data for into WT oocytes

AQP1		Ctrl	+pCMBS	+DIDS
	P \ α		α	α
Ctrl			0.0167	0.0500
+pCMBS	***P***	**4.73×10^{-5}**		0.0250
+DIDS	***P***	0.361	**0.00483**	

Statistics Table 9*D* Statistics summary of channel-specific P_f data for into AQP1-FLAG oocytes

AQP1-FLAG		Ctrl	+pCMBS	+DIDS
	P \ α		α	α
Ctrl			0.0167	0.0500
+pCMBS	*P*	**7.49×10^{-8}**		0.0250
+DIDS	*P*	0.322	**1.25×10^{-4}**	

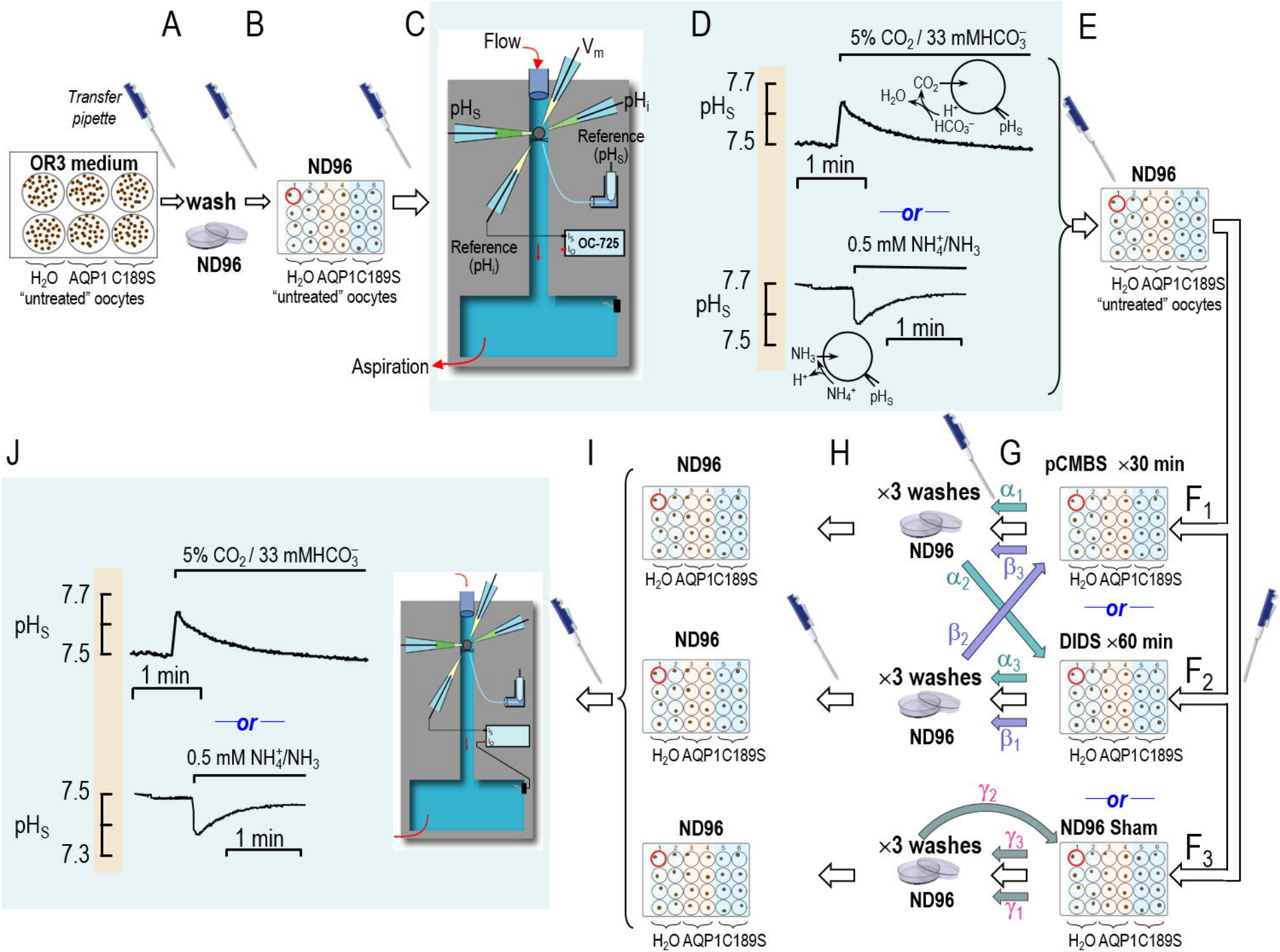
A
B
C
D
E
Transfer pipette
OR3 medium
wash
ND96
H2O AQP1 C189S
"untreated" oocytes
ND96
H2O AQP1C189S
"untreated" oocytes
Flow
Vm
pHS
pHi
Reference (pHS)
Reference (pHi)
OC-725
Aspiration
5% CO2 / 33 mMHCO3−
7.7
pHS
7.5
1 min
CO2
H2O
H+
HCO3−
pHS
or
0.5 mM NH4+/NH3
7.7
pHS
7.5
1 min
NH3
H+
NH4+
pHS
ND96
H2O AQP1C189S
"untreated" oocytes
J
I
H
G
5% CO2 / 33 mMHCO3−
7.7
pHS
7.5
1 min
or
0.5 mM NH4+/NH3
7.5
pHS
7.3
1 min
ND96
H2O AQP1C189S
ND96
H2O AQP1C189S
ND96
H2O AQP1C189S
×3 washes
ND96
×3 washes
ND96
×3 washes
ND96
α1
β3
α2
β2
α3
β1
γ2
γ3
γ1
pCMBS ×30 min
H2O AQP1C189S
F1
or
DIDS ×60 min
H2O AQP1C189S
F2
or
ND96 Sham
H2O AQP1C189S
F3

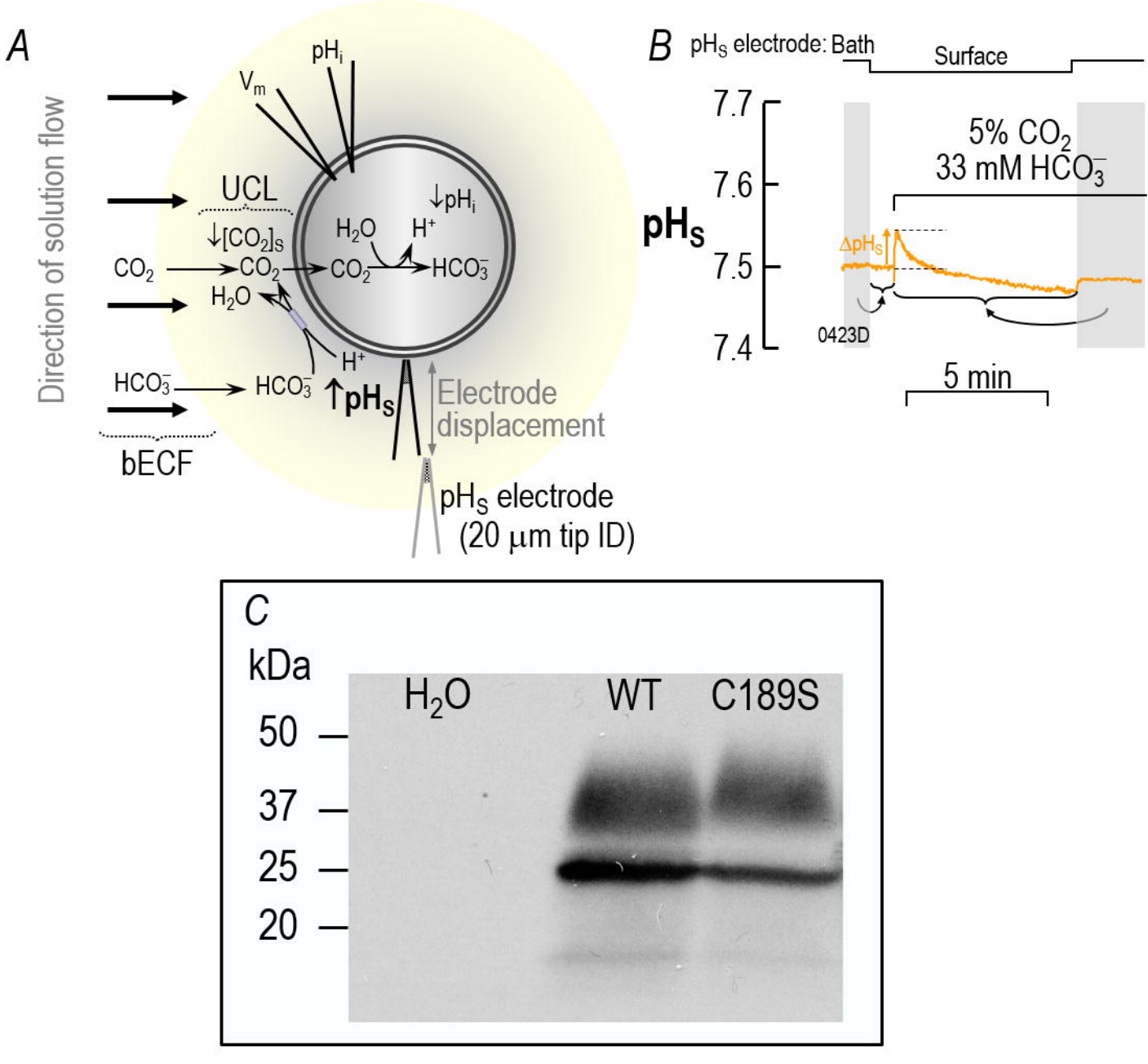
A
Direction of solution flow
pHi
Vm
UCL
↓pHi
↓[CO2]S
H2O
H+
CO2
CO2
CO2
HCO3−
H2O
H+
HCO3−
HCO3−
↑pHS
Electrode displacement
bECF
pHS electrode (20 μm tip ID)
B
pHS electrode: Bath
Surface
7.7
7.6
7.5
7.4
pHS
5% CO2
33 mM HCO3−
ΔpHS
0423D
5 min
C
kDa
H2O
WT
C189S
50
37
25
20

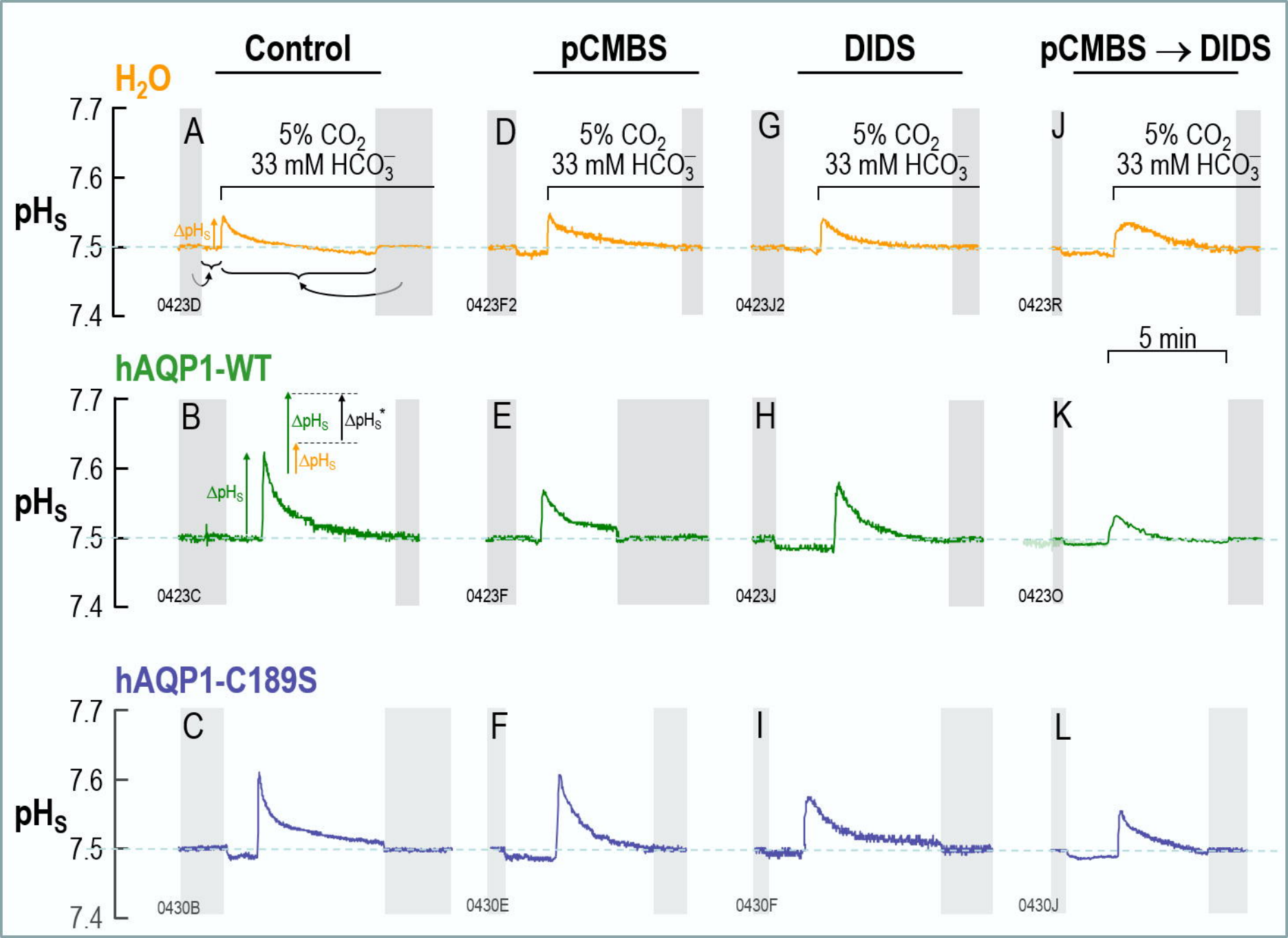
Control
pCMBS
DIDS
pCMBS → DIDS
H2O
hAQP1-WT
hAQP1-C189S
pHS
7.7
7.6
7.5
7.4
A
B
C
D
E
F
G
H
I
J
K
L
5% CO2
33 mM HCO3−
ΔpHS
ΔpHS*
5 min
0423D
0423F2
0423J2
0423R
0423C
0423F
0423J
0423O
0430B
0430E
0430F
0430J

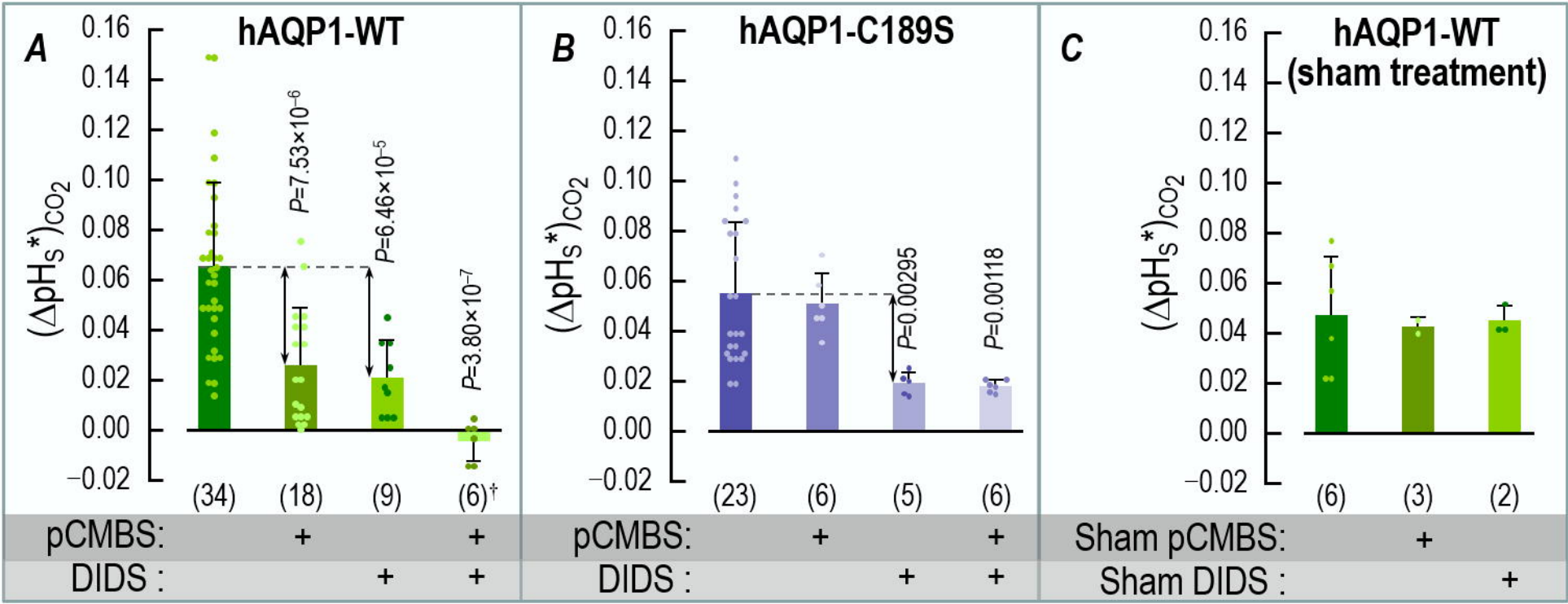
A
hAQP1-WT
B
hAQP1-C189S
C
hAQP1-WT
(sham treatment)
$(\Delta pH_S^*)_{CO_2}$
0.16
0.14
0.12
0.10
0.08
0.06
0.04
0.02
0.00
−0.02
P=7.53×10−6
P=6.46×10−5
P=3.80×10−7
P=0.00295
P=0.00118
(34)
(18)
(9)
(6)†
(23)
(6)
(5)
(6)
(6)
(3)
(2)
pCMBS:
DIDS :
Sham pCMBS:
Sham DIDS :
+

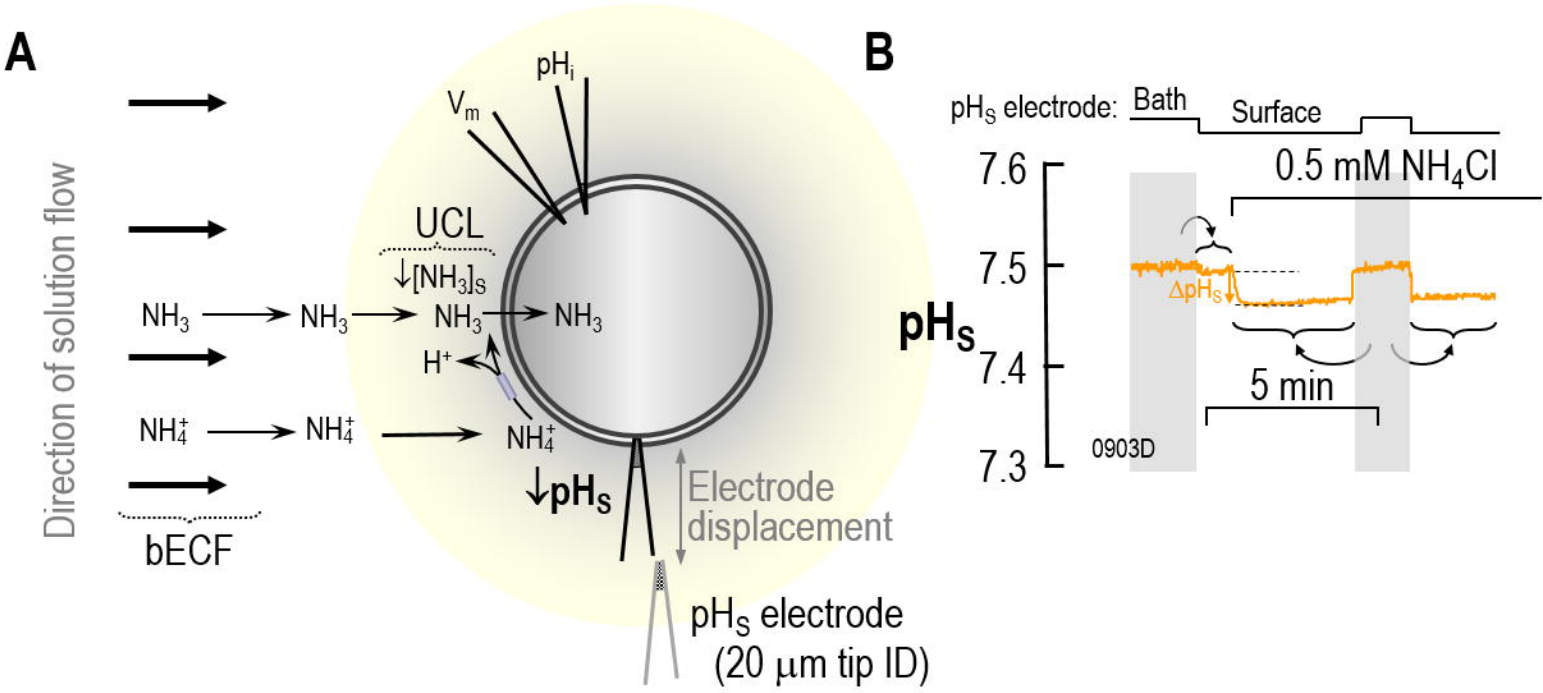
A
Direction of solution flow
bECF
UCL
↓[NH3]S
NH3
NH3
NH3
NH3
H+
NH4+
NH4+
NH4+
↓pHS
Vm
pHi
Electrode displacement
pHS electrode
(20 μm tip ID)
B
pHS electrode:
Bath
Surface
0.5 mM NH4Cl
7.6
7.5
7.4
7.3
pHS
ΔpHS
5 min
0903D

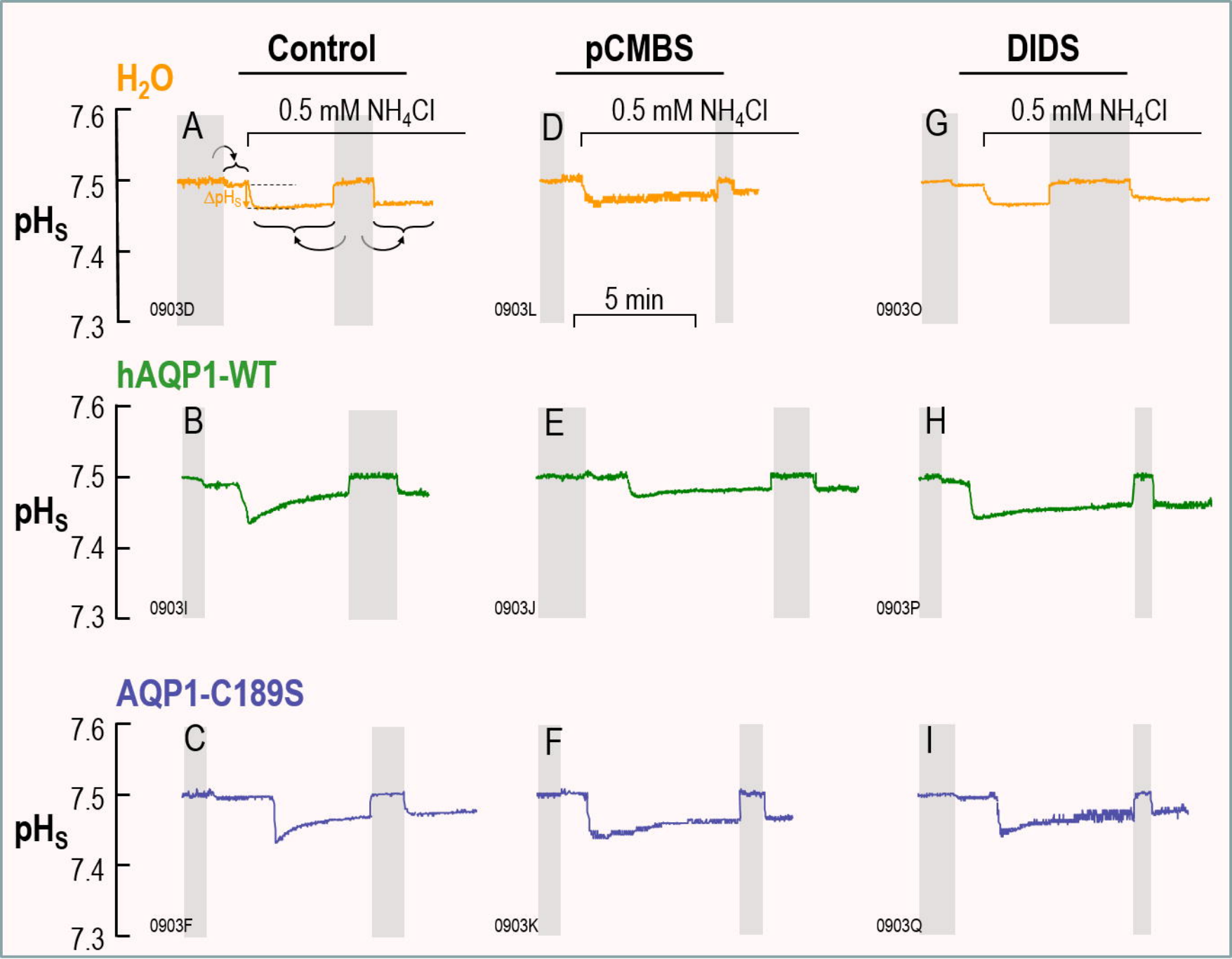
Control
pCMBS
DIDS
H2O
hAQP1-WT
AQP1-C189S
0.5 mM NH4Cl
0.5 mM NH4Cl
0.5 mM NH4Cl
A
B
C
D
E
F
G
H
I
ΔpHs
pHs
7.6
7.5
7.4
7.3
5 min
0903D
0903I
0903F
0903L
0903J
0903K
0903O
0903P
0903Q

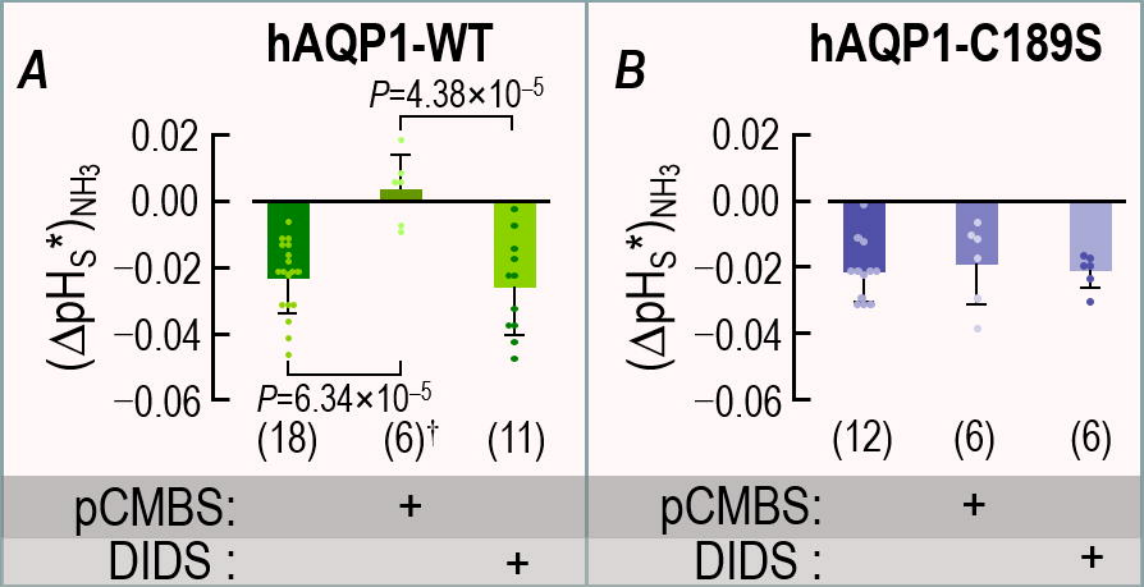
A
hAQP1-WT
P=4.38×10−5
0.02
0.00
−0.02
−0.04
−0.06
(ΔpHS*)NH3
P=6.34×10−5
(18)
(6)†
(11)
pCMBS:
+
DIDS :
+
B
hAQP1-C189S
0.02
0.00
−0.02
−0.04
−0.06
(ΔpHS*)NH3
(12)
(6)
(6)
pCMBS:
+
DIDS :
+

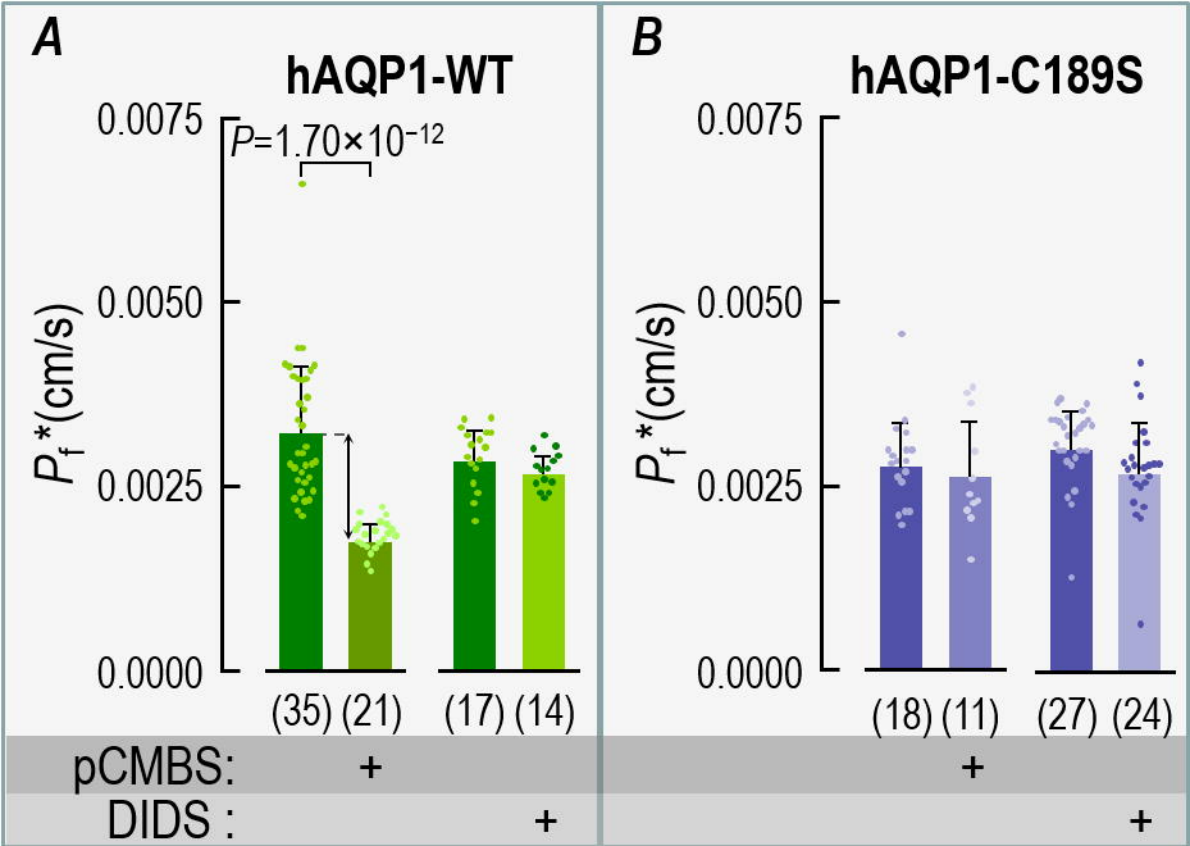
A
hAQP1-WT
P=1.70×10−12
0.0075
0.0050
0.0025
0.0000
Pf*(cm/s)
(35) (21) (17) (14)
pCMBS: + +
DIDS : + +
B
hAQP1-C189S
0.0075
0.0050
0.0025
0.0000
Pf*(cm/s)
(18) (11) (27) (24)
+ +

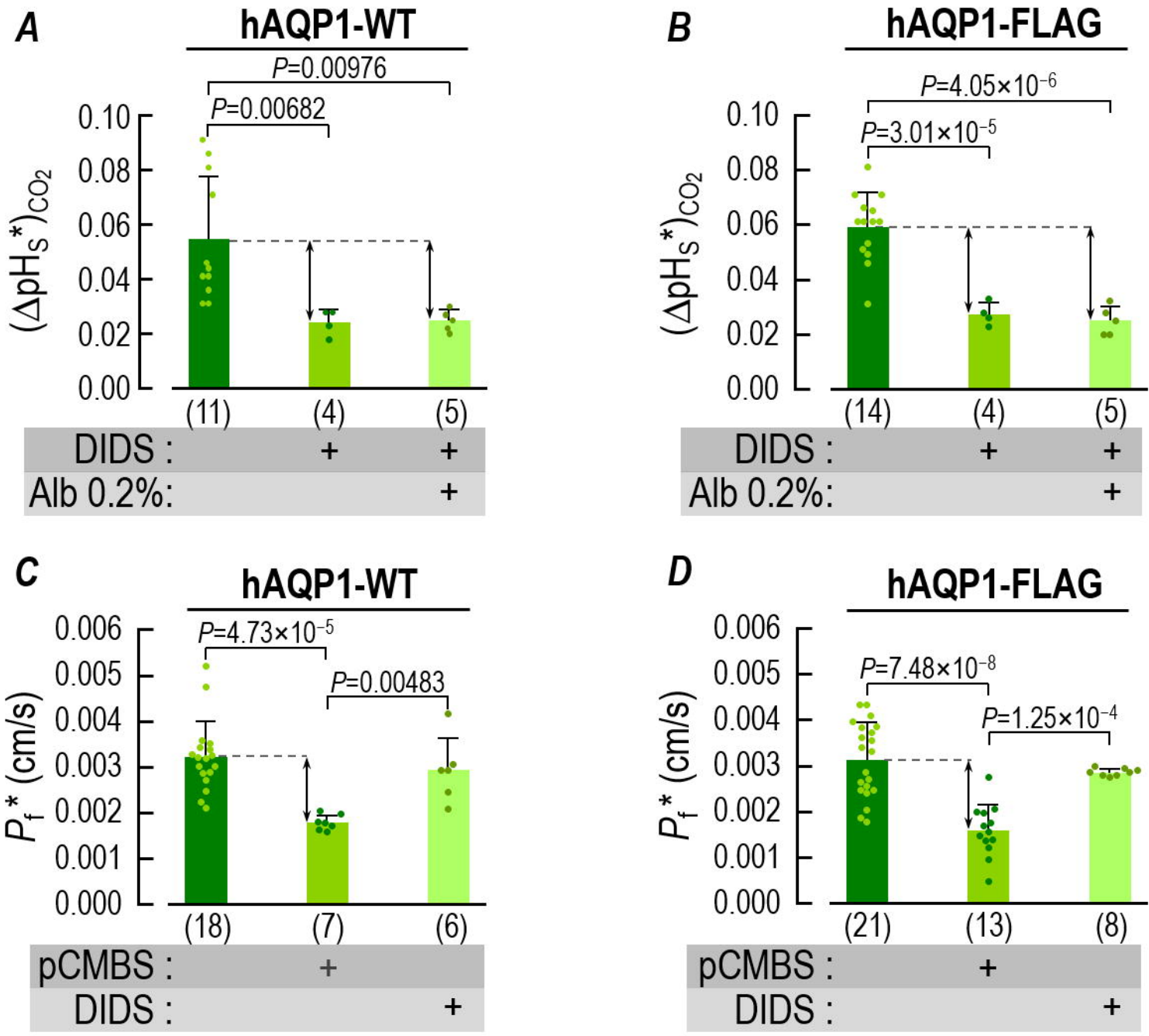
A
hAQP1-WT
P=0.00976
P=0.00682
0.10
0.08
0.06
0.04
0.02
0.00
(ΔpHS*)CO2
(11)
(4)
(5)
DIDS :
+
+
Alb 0.2%:
+
B
hAQP1-FLAG
P=4.05×10−6
P=3.01×10−5
0.10
0.08
0.06
0.04
0.02
0.00
(ΔpHS*)CO2
(14)
(4)
(5)
DIDS :
+
+
Alb 0.2%:
+
C
hAQP1-WT
P=4.73×10−5
P=0.00483
0.006
0.005
0.004
0.003
0.002
0.001
0.000
Pf* (cm/s)
(18)
(7)
(6)
pCMBS :
+
DIDS :
+
D
hAQP1-FLAG
P=7.48×10−8
P=1.25×10−4
0.006
0.005
0.004
0.003
0.002
0.001
0.000
Pf* (cm/s)
(21)
(13)
(8)
pCMBS :
+
DIDS :
+

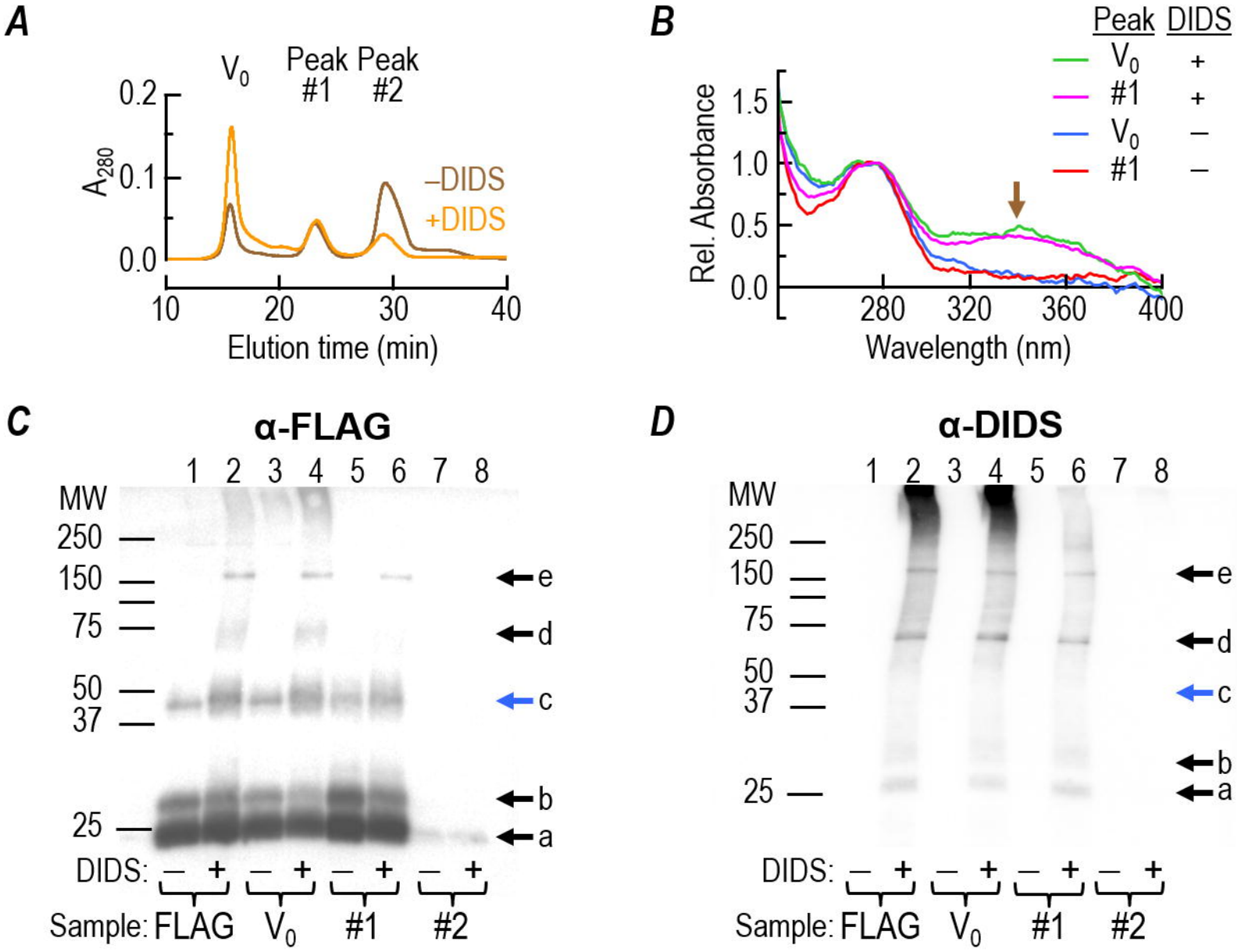
A
V0
Peak #1
Peak #2
0.2
0.1
0.0
A280
–DIDS
+DIDS
10
20
30
40
Elution time (min)
B
Peak
DIDS
V0 +
#1 +
V0 –
#1 –
1.5
1.0
0.5
0.0
Rel. Absorbance
280
320
360
400
Wavelength (nm)
C
α-FLAG
1 2 3 4 5 6 7 8
MW
250
150
75
50
37
25
e
d
c
b
a
DIDS: – + – + – + – +
Sample: FLAG V0 #1 #2
D
α-DIDS
1 2 3 4 5 6 7 8
MW
250
150
75
50
37
25
e
d
c
b
a
DIDS: – + – + – + – +
Sample: FLAG V0 #1 #2